MICROTECHNOLOGY FOR SPATIAL AND TEMPORAL CONTROL OF GENE EXPRESSION IN DEVELOPING EMBRYOS AND CELLS

by

Tushar Bansal

A dissertation submitted in partial fulfillment
of the requirements for the degree of
Doctor of Philosophy
(Electrical Engineering)
in the University of Michigan
2009

Doctoral Committee:

        Assistant Professor Michel M. Maharbiz, Co-Chair
        Associate Professor Euisik Yoon, Co-Chair
        Professor Cunming Duan
        Professor Kensall D. Wise

To my family

Acknowledgements

I would like to express my most sincere and deepest gratitude to all those who have provided me support and encouragement during my Ph.D process. I would like to thank my advisor, Dr. Michel M. Maharbiz for his guidance, assistance and overall mentoring during my research. His great enthusiasm for innovation, dedicated work ethic and insightful perspective are a great source of inspiration to me and I will carry them for the rest of my career and life.

I thank my committee co-chair, Dr. Euisik Yoon for agreeing to be my co-chair. I also want to give special thanks to Dr. Cunming Duan for being a great collaborator and providing his vast expertise and experience in developmental biology towards zebrafish research in my thesis. I also want to thank Dr. Kensall Wise for agreeing to be on my committee on such a short notice and Yogesh B. Gianchandani, for lending me his time, experience and asking some insightful questions during my prelim exam. My gratitude also goes out to the Wise/Najafi Laboratory and Neural Engineering Laboratory for providing resources and assistance for my experimental setup. I also want to thank the staff of WIMS ERC and SSEL/LNF for creating a superb environment to carry out my research (Ning Gulari, Kimberly Appel, Tim Brock, Gregory Allion, Terre Briggs, Phil Collica, Sandrine Martin, Edward Tang, Brian VanDerElzen). They are the real unsung heroes of this process.

TABLE OF CONTENTS

List of Figures

List of Tables

List of Appendices

CHAPTER I

INTRODUCTION

Much of the biology in multicellular development depends upon the exchange of messages between cells: by exchanging chemical or mechanical information, cells influence the state of other cells near them and act in a coordinated fashion. Many tissue patterning events such as migration, proliferation, development and differentiation that occur *in vivo*, occur in relation to changes in local microenvironment of a cell. Such events can be attributed to reactions triggered by neighboring cells or concentration dependent effects introduced via signaling molecules, forcing a cell to choose between various available developmental pathways. By choosing one pathway over another, a cell undergoes changes and influences other cells during its transition. The cumulative effect of such cycles occurring locally leads to the emergence of structural patterns within a developing organism. The ability to regulate cells by controlling their local microenvironment through engineered interfaces will aid in the study of such developmental processes in a more advanced manner. The work presented in this thesis focuses on the design, fabrication and results of microfabricated interfaces for the patterned delivery of foreign molecules and gene constructs into developing embryos and cells (Figure 1.1).

1.1 Spatiotemporal cell signaling and tissue patterning

Spatiotemporal signals are important regulators of cell positioning and behavior [1, 2]. During development, these signals play a central role in the orchestration of cell proliferation, communication and differentiation which eventually gives rise to distinctive shapes, forms and functions in organisms of all scales [3, 4]. In developmental biology, the concept of morphogen (or 'form-generating substance') has been researched for several decades to explain how, during organism development, cells can determine their positions within a homogeneous field, and consequently adopt appropriate fates during tissue patterning and structuring [1, 5]. Morphogens induce coordinated growth and differentiation of several different cell types along a gradient, generating the normal neighbor relationships of a functional organ. Briefly, a source secretes morphogen ligands which diffuse away from the source and create a declining chemical gradient. Cells experiencing morphogen concentrations above a certain threshold choose a different developmental pathway (express high threshold target genes only) than the ones below the threshold i.e. experiencing lower concentrations. Such immediate cellular level responses propagate into a sequence of more differentiated responses at higher levels and eventually result in phenotype changes to the overall structure [6, 7, 8]. For example, the Biocoid (Bcd) gradient in early *Drosophila melanogaster* embryos is one of the most studied morphogens [6, 9, 10] and controls the anterior-posterior (AP) patterning of the developing embryo, especially the head structures. A high concentration of Bicoid at the anterior pole of the embryo leads to the expression of the *hunchback* gene [1] while a high concentration of Nanos at the posterior pole leads to the formation of abdominal segments due to the expression of the *caudal* gene. Other examples include morphogen
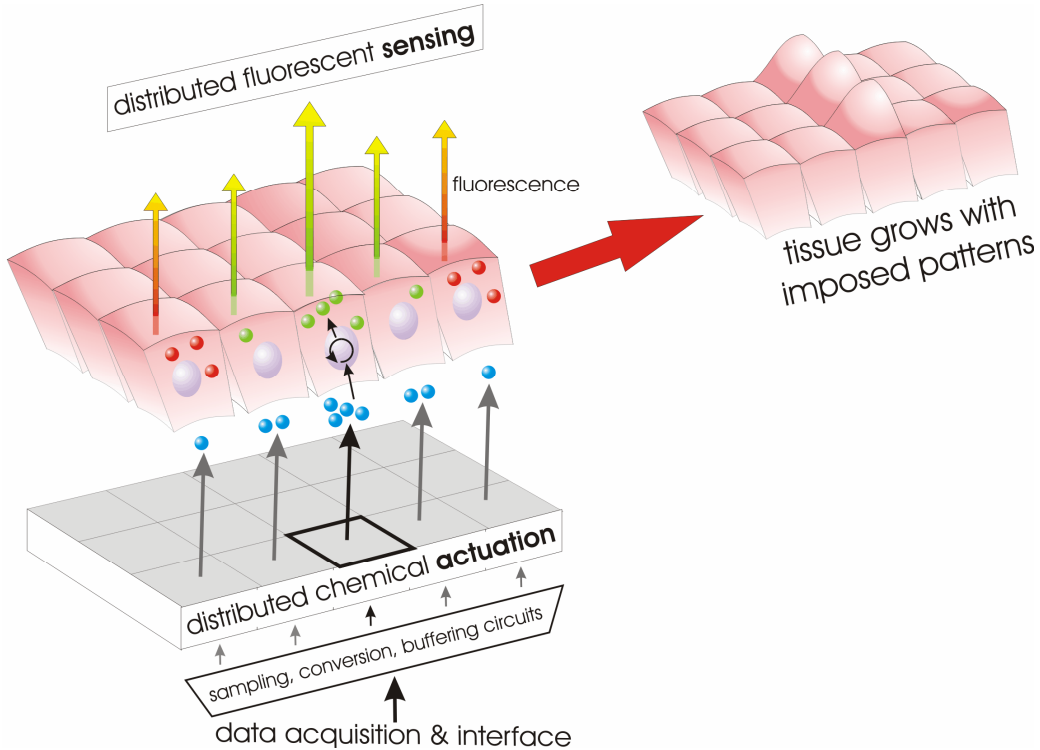
Figure 1.1: The objective of this work is to develop bio-interface microtools (as shown in the grey block) which can interface with developing systems and control spatial and temporal developmental patterns in them.

gradients of TGF beta family members, Vg1 and activin, which have been shown to act as secreted morphogens and define the mesoderm formation and patterning in adult Xenopus [11]. In this case, they even act as relays for signal propagation to distant cells. Such a complex sequence of events depends upon the appropriate spatial and temporal coordination of numerous interactions between cells and their neighbors, the surrounding extracellular matrix (ECM), soluble and diffusible factors and other local physical forces.

1.2 Current research with bio-interface systems

To carry out well-controlled research using cells, the microenvironment in which the cells live must be well defined and controlled. Traditionally, culture dishes have been

utilized to study cells in different environments which have proved both difficult and unreliable to generate stable gradations of the local microenvironment. The usual methods (injection or embedding a bead of morphogen) are time-consuming, prone to positioning errors and tissue damage, and generate very limited gradients as common morphogens are simply added globally to cell cultures. This lack of ability to accurately control a cell's microenvironment brings forward a pressing need across much of biomedical research for techniques that can control the patterning of chemical gradients. Such techniques can greatly aid in the study of cell differentiation, neuronal growth, microbial sensing and microbial consortia [12, 13, 14, 15].

Micro-ElectroMechanical-Systems (MEMS) and microfluidic devices are beginning to find applications within biology as they provide a powerful new set of tools to control and manipulate cells [16, 17, 18]. Because of the length scales involved, spatial and temporal organization of cellular signals can be appropriately studied with some emerging technologies that control the diffusible environment in developing tissues [14, 16, 17, 18]. Among these technologies, soft lithography patterning using elastomer (mechanically soft) materials is the most common [17, 19]. Takayama *et al.* were the first to demonstrate localized perturbation of selected subcellular microdomains with membrane-permeable molecules in a single cell using soft lithography with laminar flow techniques [16]. By allowing different solutions to flow from different inlets at low velocity, parallel streams were created in the main channel and a single bovine endothelial cell was perturbed at local regions to study intracellular molecular kinetics. More recently, Ismagilov *et al.* have demonstrated the implementation of microfluidic techniques to perturb embryonic development in order to study the effects of temperature

4

variations in localized areas of a growing embryo [20]. Two halves of a *Drosophila* embryo were exposed to different water temperatures and were observed to develop at different rates [20]. However, when the temperature change was removed sufficiently early, the embryo resynchronized the two halves and proceeded to develop normally. These recent findings and approaches signal a slow shift away from conventional cell control studies and more towards understanding processes which regulate developing organisms.

1.3 Growing needs in developmental biology

Additionally, there has been a considerable interest mounting in the patterned chemical intervention of developing organisms [21]. The ability to modify spatiotemporal gene expression in two (or three) dimensions via patterned delivery of genes, proteins and bioactive molecules would allow for more biologically-relevant manipulations of developing systems. For example, Voiculescu *et al.* [22, 23] recently demonstrated spatial-temporal control of DNA and morpholino oligonucleotide (MO) doses in selected regions of early chick embryos with a custom electroporation setup made from hand-modified platinum wires and inserted into an acrylic fixture. Several new chemical methods, such as the tetracycline, dexamethasone and insect hormone regulated gene expression systems would benefit from a method which provides patterned delivery of trigger compounds into developing embryos [24]. Similarly, simultaneous delivery of multiple molecules in different patterns would also expand the type of experiments performed in spatially heterogeneous systems, particularly where multiple pathways with specific timings are involved [21, 25, 26]; see for example, Mara *et al.* [27] which

demonstrates zebrafish somitogenesis is governed by a segmentation clock that generates oscillations in expression of several Notch pathway genes. In this system, chevron-shaped areas of gene expression within the tailbud demarcate where the clock is set up in the progenitor cells (priming), where the clock starts running (initiation), and where the clocks of neighboring cells are entrained (synchronization).

Utilizing such interfaces, future experiments may enable the understanding of the mechanisms responsible for robustness of development and may uncover the limits beyond which developmental programs cannot be perturbed.

1.4 Thesis organization

In this work, we present the design, fabrication and results of microfabricated interfaces for the patterned delivery of foreign molecules via diffusion and electroporation into developing embryos. These systems were used to 'draw' two-dimensional spatial patterns of tracer molecules and provide pixel-style array (Figure 1) delivery of DNA and mRNA into the yolk and cells of zebrafish embryos (*Danio rerio*) at different stages of development. The successful delivery of two-dimensional patterns of trypan blue (normal dye), texas red (fluorescent dye), pCS2eGFP DNA and GFP-mRNA in both chorionated and dechorionated embryos is also demonstrated. Both DNA and mRNA were expressed in the desired patterns subsequent to delivery.

Chapter II gives a brief overview of zebrafish emergence as the new model organism for experimental research and study. Zebrafish developmental cycle is briefly described and characteristics of the membrane are discussed.

Chapter III describes the various techniques that are currently utilized to introduce extracellular compounds into developing embryos and discusses their advantages and disadvantages.

Chapter IV presents the design, fabrication and characterization of electrostatic actuators and their application as dosing devices and low voltage microfluidic valves. Micropores can be used to dynamically regulate microenvironments in a cell.

Chapter V demonstrates the combination of electroporation and microfluidics (without microinjection) to deliver foreign compounds into zebrafish embryos with specific patterns in localized regions. The efficacy of the device is demonstrated by using dechorionated and chorionated as well as young (3 hpf) and old (24 hpf) embryos as measured in hours post fertilization (hpf).

Chapter VI presents the future work consisting of electroporation spatial gene constructs into bacterial cell colonies. Construction of synthetic modules to immobilize bacterial cell colonies and deliver different genes to study their evolution and stability is proposed.

1.5 Summary

The idea of locally secreted signals that act as morphogens and directly pattern a tissue by eliciting distant responses has been an attractive mechanism to explain many developmental events [1, 2, 3]. We are interested in controlling the chemical microgradients that lead to differentiation and morphogenesis in tissue and primary cells. This type of control or essentially 'hacking' the developmental program of an organism

requires microsystems with cell diameter dosing resolutions and is possible with the technology we present.

We believe that the ability to modify two dimensional specially-shaped areas in developing organisms with controlled delivery of genes and proteins in spatially patterned shapes would allow more biologically-relevant manipulations of a complete system's development [21]. Such control or 'hacking' tools are limited at this time and our technology will provide an additional biological tool. Similarly, simultaneous delivery of multiple molecules in different patterns would also expand the type of experiments performed in spatial and temporal heterogeneous systems, particularly where multiple pathways with specific timings are involved [21, 25, 26].

CHAPTER II

OVERVIEW OF ZEBRAFISH

Over the past 25 years, the zebrafish (*Danio rerio*) has become a powerful model system for the investigation of vertebrate development, physiology and gene function due to a number of advantageous features: zebrafish represent a vertebrate system; zebrafish embryos are transparent and develop outside the parent, eliminating the complication of maternal compensation; a large number of eggs are laid at a time; and all self sustaining proteins and chemicals are present within the yolk. Transparency of the developing embryo is particularly well suited for tracing the movement of individual cells and how extrinsic and intrinsic factors act together to regulate embryonic development and growth. Additionally, the zebrafish nervous system is relatively simple and starts functioning within 24 hours.

This chapter discusses zebrafish as a new model system and briefly explores its various developmental stages. Additionally, the fluid mosaic model for membranes is briefly touched upon and its relevance to the research presented in this thesis is briefly explored.

2.1 Introduction

Model organisms are highly valued by researchers investigating developmental biology - the transformation of an organism from a fertilized egg into an adult. A 'model'

organism is a simple species that is extensively studied to understand its biological phenomena. Once understood, this knowledge is further applied towards understanding other species. Traditionally, many of the fundamental principles of vertebrate embryology were revealed by experiments in amphibian and avian embryos [28]. One of the most famous of such model organisms has been the common fruit fly (*Drosophila melanogaster*), which has been used for nearly a century and has a rich history of research behind it [29 - 32], but remarkable insights have also come from studies of frogs, chicks, worms and mice [33 - 36]. However, a clear understanding of underlying mechanism of development has been hampered due to the inability to carry out rapid genetic studies in such organisms [28].

2.2 Zebrafish as a new model system

In more recent times, the zebrafish has emerged as an excellent model system for understanding vertebrate neural development because of its high degree of similarity to mammals in molecular mechanisms of developmental and cellular physiology [37, 38]. The nervous system in vertebrates is extremely specific and precise. It requires the production of specific cell types, at precise times, in exact proportions, and connections between those cell types to produce an accurately functioning system. The embryonic zebrafish has an accessible and relatively simple nervous system, with many of its components formed and functioning as early as 24 hours post fertilization (hpf). The use of mutagenesis screens in the vertebrate zebrafish model to understand the development of the nervous system allows researchers the opportunity to identify molecules that could not otherwise be found by using other vertebrate systems [28].

Zebrafish embryos are large, robust, transparent and develop externally to the mother, thus providing unique advantages towards experimental observation and manipulation. Embryo transparency allows researchers to track cell organization, observe gene functionality and understand biological pathways. With high fertility rates, a three month generation time, sequenced genome, thousands of mutant lines established and sophisticated molecular, genetic and imaging techniques available, the zebrafish is now a well-established model system.

Figure 2.1   **Zebrafish (*Danio rerio*) has emerged as an excellent model system in developmental biology. a) Fertilized zebrafish developing embryos are transparent and protected by an outer chorion. b) Adult zebrafish with stripes.**

2.3 Zebrafish developmental cycle

The basic vertebrate body plan of the zebrafish embryo is established in the first 10 hours of development. This period is characterized by the formation of the anterior-posterior and dorsal-ventral axes, the development of the three germ layers, the specification of organ progenitors, and the complex morphogenetic movements of cells. Broadly, the zebrafish embryogenesis can be divided into seven periods – the zygote, cleavage, blastula, gastrula, segmentation, pharyngula and hatching periods. Periods are

further divided into stages and highlight the changes in developmental morphologies in the first 3 days of fertilization. Discussion of these stages is important as introduction of extracellular compounds at different stages yield different results. Below, some of the significant events that occur during these periods are described. A thorough review and description of these processes can be found elsewhere [39]. A complete zebrafish development cycle is shown at the end of the section.

2.3.1 Zygote period (0 - $\frac{3}{4}$ h)

The newly fertilized egg is considered to be in the zygote stage. It has only one cell until cleavage occurs about 40 minutes after fertilization [39]. During cleavage, the cell starts dividing into more cells.

2.3.2 Cleavage period ($\frac{3}{4}$ - $2\frac{1}{4}$ h)

During the cleavage period, the zygote undergoes a meroblastic (only partial undercut of the blastodisc) cell division process. The division occurs at about 15 minute intervals producing a cluster of 64 cells which add up to be the same size as the original zygote. In the cleavage period, these cells are known as blastomeres.

2.3.3 Blastula period ($2\frac{1}{4}$ - $5\frac{1}{4}$ h)

At the start of the blastula period, the embryo has 128 cells and starts resembling a ball-shape. In this period, the embryo enters the midblastula transition (MBT), the yolk syncytial (YSL) layer is formed and epiboly begins. MBT sets in at the 512 cell-stage and is marked by asynchronous cell cycle lengthening. During cycle 10 (~1k cells) [40, 41], the marginal cells lying against the yolk cell collapse and release their cytoplasm and

12

nuclei together into the immediately adjoining cytoplasm of the yolk cell, thereby creating the yolk syncytial layer. Late blastula period, marks the beginning of thinning and spreading of both the YSL and the blastodisc over the entire yolk cell. This process is known as epiboly.

2.3.4 Gastrula period (5 $\frac{1}{4}$ - 10 h)

During the gastrula period, cells migrate towards the interior of the blastula and their involution, convergence and extension produces the primary germ layers and the embryonic axis in the zebrafish. At 50% epiboly, a thickened marginal region called the germ ring appears during involution. Local convergence of cells at one position along the germ rings gives rise to an embryonic shield. During this event, the epiboly is temporarily stopped but continues to cover the yolk cell completely after the formation of the shield. The deep cells in the embryonic shield form two layers. The epiblast is formed at the surface and gives rise to the ectoderm. The hypoblast is formed next to the YSL and forms a mixture of endoderm and mesoderm. The end result of gastrulation is marked by an asymmetric involution of cells which forms the dorsal structures of the embryo [41].

2.3.5 Segmentation period (10 – 24 h)

During segmentation, first furrow of somites, pharyngeal arch primordia and neuromeres develop, primary organs become visible, the tail appears and there are signs of first movement. Somites are masses of mesoderm and eventually become dermis, skeletal muscle and vertebrae. The earliest few somites develop at the rate of 3 per hour for the first six and 2 per hour thereafter [42]. Primordium of initial conditions capable of triggering further growth in brain and central nervous system are satisfied as neural plate

is established and there is prominent thickness near the brain region. Around 18 hours, the tail bud begins to protrude away from the body of the embryo and the yolk appears in a kidney bean shape. At the 20-somite stage (19 hours), the length of the embryo increases, posterior trunk straightens and weak muscular contractions can be observed. The segmentation stage ends at the 26-somite stage where the two otoliths in each otic vesicle are visible with a microscope.

2.3.6 Pharyngula period (24 – 48 h)

During the pharyngula period, the body axis straightens from its early curvature about the yolk sac, set of somites gets completely developed, circulation initiates, pigmentation occurs and fins begin development. In the early pharyngula period, the embryo continues it rapid lengthening that started at 15 hours. A beating heart becomes visible at 24 hours. Pigment cells start differentiating and are prominent in the eye at 36 hours and the circulatory system is formed. Mesenchymal cells gather together to form rudimentary pectoral fin buds at 42 hours. These serve as a staging feature during the second half of this period.

2.3.7 Hatching period (48 – 72 h)

The hatching period occurs asynchronously and involves the completion of rapid morphogenesis of primary organ systems and cartilage development in the head and pectoral fin. During the hatching period, the embryo continues to grow and many developing rudiments of the pectoral fins, the jaws and the gills slowly get completed.

By the end of 72 hours, the hatched larva completes most of its morphogenesis and continues to grow rapidly. The swim bladder inflates and the anterior-dorsal protrusion of

the mouth continues. The early larva gradually begins to swim about actively and moves its jaws, opercular flaps, pectoral fins and eyes.

1 cell 0.2 h	2 cell 0.75 h	4 cell 1 h	8 cell 1.25 h
16 cell 1.5 h	32 cell 1.75 h	64 cell 2 h	128 cell 2.25 h
256 cell 2.5 h	512 cell 2.75 h	1k cell 3 h	high 3.3 h
oblong 3.7 h	sphere 4 h	dome 4.3 h	30%-epiboly 4.7 h
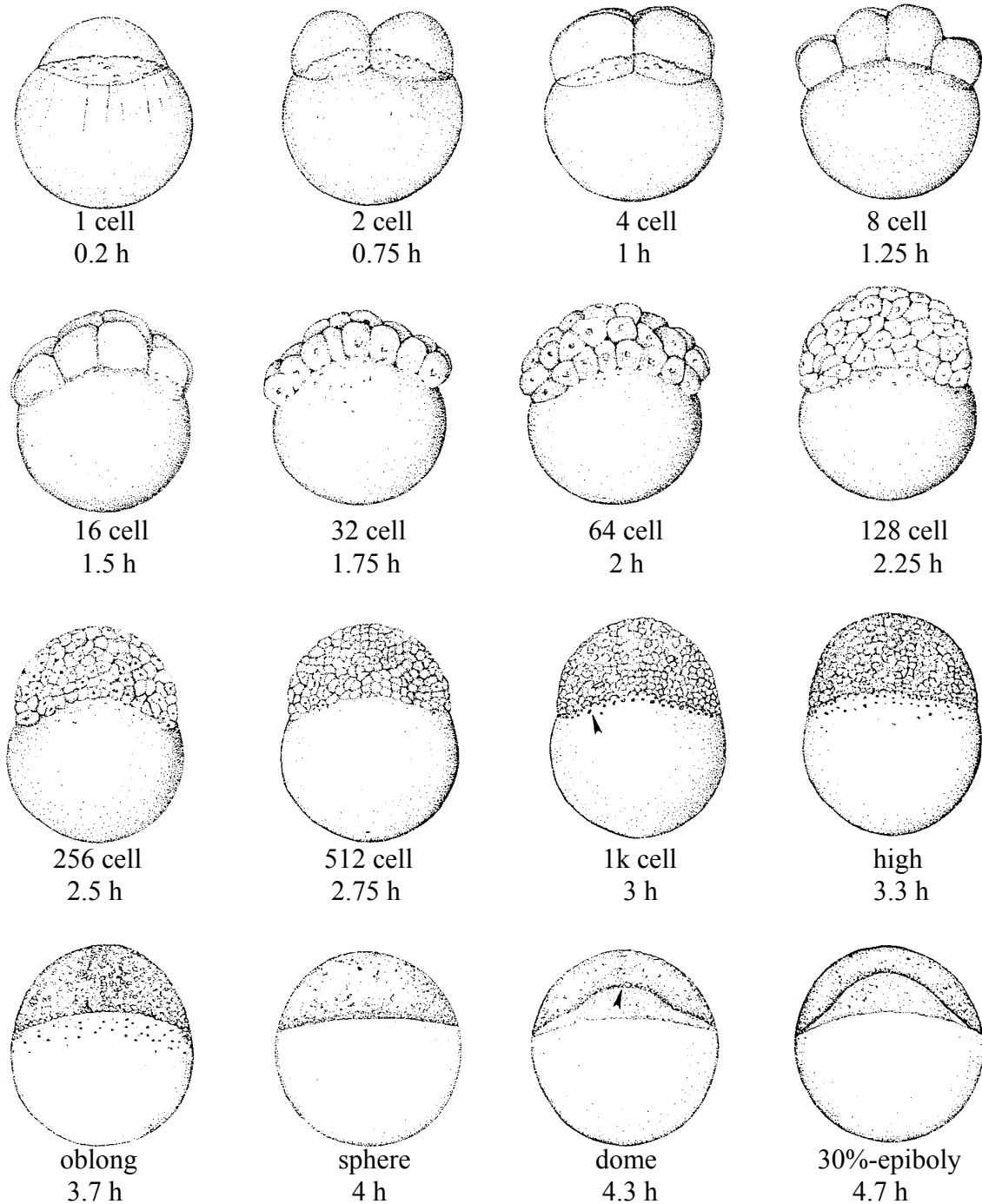
Figure 2.2: **Zebrafish development cycle at different stages defined in hours post fertilization (hpf). Adapted from Kimmel *et al.* [39].**

15
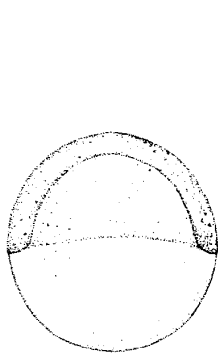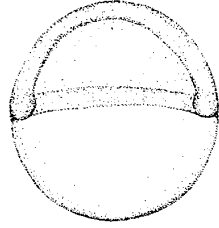
50% epiboly
5.3 h

germ ring
5.7 h
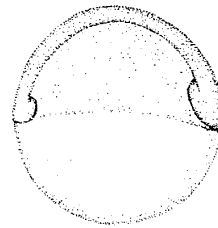
shield
6 h
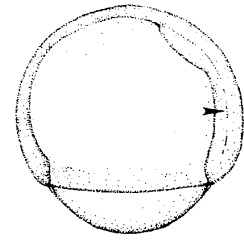
75%-epiboly
8 h
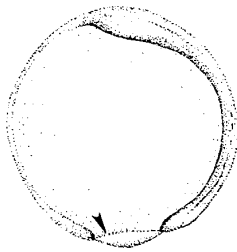
90% epiboly
9 h
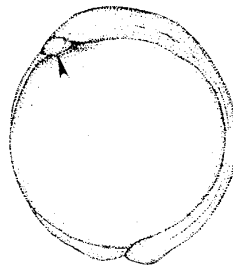
bud
10 h
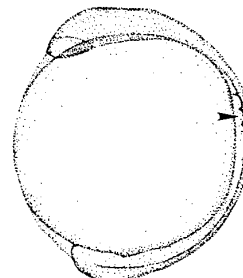
3 somite
11 h
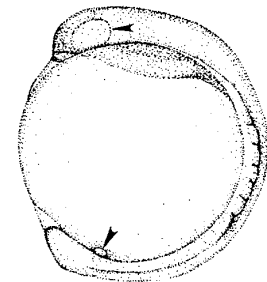
6 somite
12 h
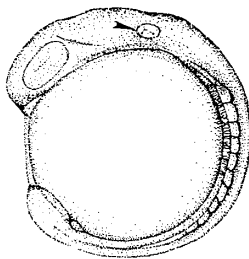
10 somite
14 h
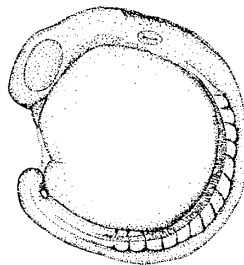
14 somite
16 h
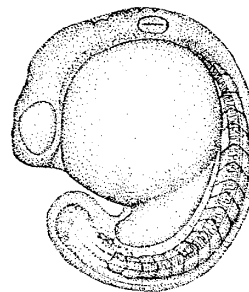
18 somite
18 h
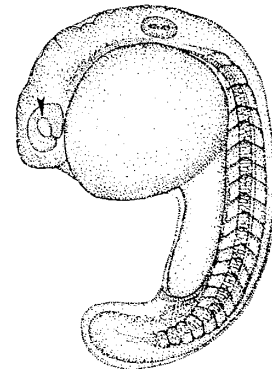
21 somite
19.5 h
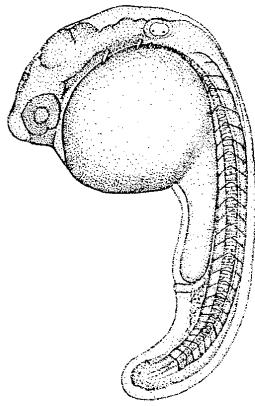
26 somite
22 h
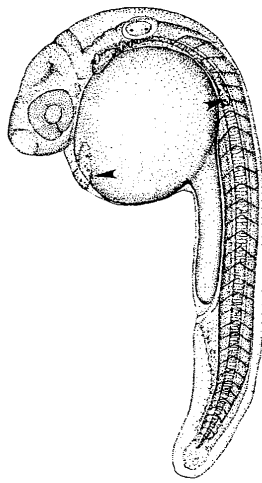
prim 6
25 h
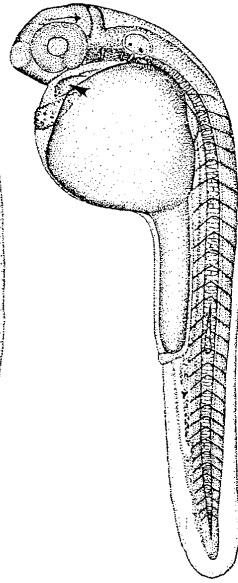
prim 16
31 h
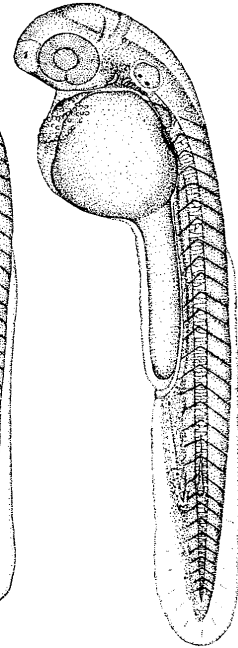
prim 22
35 h
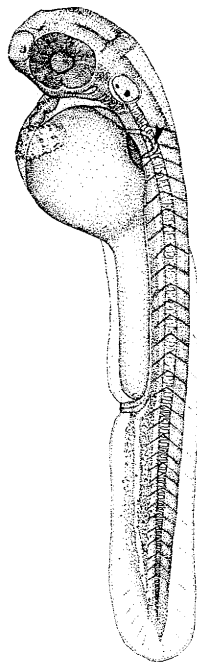
High pec
42 h
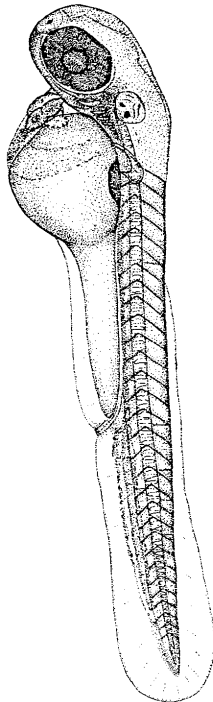
long pec
48 h
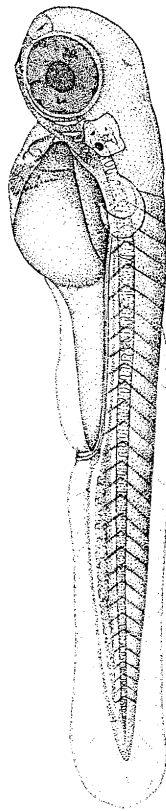
pec fin
60 h
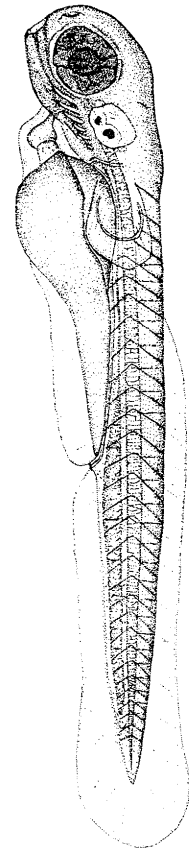
protruding mouth
72 h

2.4 Understanding membrane structure

The cell membrane acts as a porous wall to the cell and serves many functions: it protects the internal components of the cell while allowing an exchange of limited compounds with the outside world; it controls the flow of information between cells by sending and receiving electrical or chemical signals to other cells; it regulates the fluid composition within the cell by controlling the movement of fluid and other substances into and out of the cells; and some membranes are also involved in the capture and release of energy during processes like photosynthesis.

2.4.1 Membrane as a fluid mosaic model

The membrane structure is highly fluid and most of the lipid and protein molecules can move about the plane of the membrane (Figure 2.3). The fluid mosaic model of membrane structure, first proposed by S.J. Singer and G.L. Nicolson in 1972 [43], depicts the membrane as a seething mass of lipids and proteins in which movements of molecules take place in two dimensions. On one surface, chains of sugar molecules stick out and wave about. Biological membranes are thus lipid-protein-sugar 'sheet', in which the permeability barrier and structural integrity are provided by the lipids and specific functions are carried out by the proteins. The lipid and protein molecules are held together mainly by non-covalent interactions. Sugars are attached by covalent bonds to some of the lipid and protein molecules [43, 44] and provide the distinctive 'appearance'.
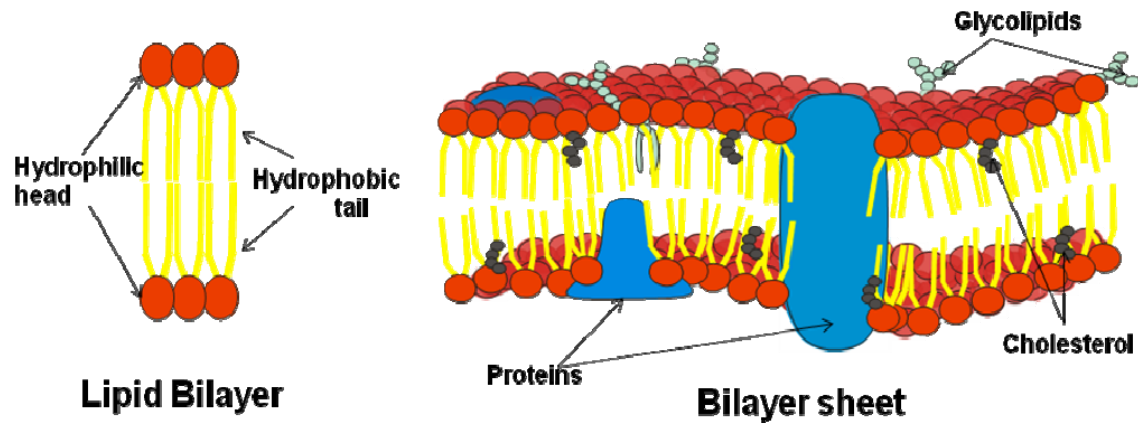
Figure 2.3: Structure of lipid bilayer. The lipid bilayer acts a restrictive barrier controlling the transport of compounds in and out of the cell.

2.4.2 Membrane transport

The phospholipid bilayer of the membrane with its charged heads and hydrophobic core is very selectively permeable. Two types of transport proteins help in the crossing of particles through cell membranes. Channel proteins form water filled pores across the bilayer, through which inorganic ions move in single files. Carrier proteins bind specific molecules or ions and transfer them across the membranes.

Molecules such as sugars, amino acids and inorganic ions are both actively and passively transported across a cell membrane due to concentration gradient. During passive transport no input energy is required as molecules move from a region of high concentration to a region of low concentration. This normal process of diffusion is sometimes facilitated by membrane proteins. Small hydrophobic molecules can readily cross this through simple diffusion by dissolving in the hydrophobic core. In order to transport a molecule against the electrochemical concentration gradient, cells require extra energy and the process is called active transport. This extra energy can be provided to the membrane in the form of externally provided electrical or thermal energy.

19

2.4.3 Zebrafish membrane

Zebrafish embryos have rectifying membranes that allow water to leave but not reenter readily. This is assumed to be an evolutionary trait that allows freshwater embryos to grow in hypoosmotic environments without osmoregulatory organs [45].

A zebrafish embryo is composed of two structures: the outer chorion and the inner yolk with cells. The principal role of the chorion is physical protection of the embryo while allowing a two way movement of water and solutes. Additionally, two distinct membrane complexes are recognized: the outer chorion and the inner plasma (vitelline) membrane. The plasma membrane and the underlying syncytial layer are considered to be the main permeability barrier. Studies confirm that the outer chorion membrane complex is 1.5 – 2.5 µm in thickness [45, 46] and consists of three layers, electrondense outer and innermost layers 0.2-0.3 µm and 1.0-1.6 µm in thickness respectively) separated by an electron-lucent middle layer (0.3-0.6 µm in thickness). The syncytial layer is 1-4 µm thick beneath the plasma membrane. All these membranes combine to provide a strong permeability barrier to zebrafish and have been areas of numerous studies [47-49].

2.5 Conclusion

In brief, the zebrafish attracts researchers because (*a*) it is a vertebrate with simple husbandry requirements, (*b*) it is relatively fecund and generates clutches of 100–200 embryos weekly, (*c*) its fertilization and development are external, and (*d*) its embryo is transparent. The outer chorion and YSL act as permeability barriers and are only permeable to small hydrophobic solutes and impermeable to inorganic compounds and ionic molecules.

CHAPTER III

BACKGROUND TECHNOLOGY

The ability to introduce, remove, or modify compounds in the intracellular environment of a cell is pivotal towards understanding cellular structure and function. By tracing the pathway of tracer dyes or biomolecules, cellular communication and various developmental mechanisms can be studied and understood in developing organisms [50 - 56]. However, the transport of extracellular compounds into a cell is prevented by the cell membrane which surrounds the cell, gives it structure and acts as a restrictive barrier as discussed in Chapter II. Being selectively permeable, cell membrane controls the movement of substances in and out of a cell.

Various techniques exist to increase the permeability of the cell membrane and deliver compounds inside the cell. This chapter gives an overview of different techniques which currently exist to deliver extracellular compounds into developing embryos, especially zebrafish.

3.1 Microinjection

Microinjection remains one of the oldest techniques to introduce foreign compounds for probing cellular and molecular development inside a cell [57, 58, 59]. Microinjection refers to the process of using a very fine needle (typically a drawn glass

capillary) to insert compounds at a microscopic level into living cells. It is a simple mechanical process in which a needle, roughly 0.5-5 μm in diameter penetrates the cell membrane. The desired compounds are then injected into the cytoplasm with an air pressure and the needle is removed. These compounds can then be visually traced overtime as cellular changes occur, providing an insight into cellular functioning
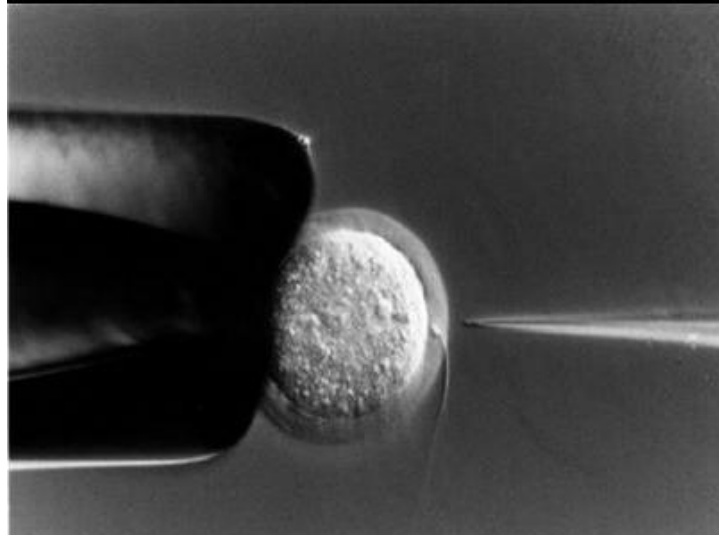
Figure 3.1:   A typical microinjection setup is shown. During microinjection, a cell is placed in an agar petri dish and a very fine glass needle (0.5 – 5μm diameter) is manually inserted into the cell to inject extracellular compounds in it.

[60, 61]. The technique is frequently used to insert biomolecules such as DNA, mRNA and RNAi into single cells [62, 63]. Nowadays, microinjection is normally performed under a specialized optical microscope setup called a micromanipulator and uses pressurized injections.

Microinjection is the most effective technique in terms of preventing cell damage, cell viability and cell waste, and is the most widely used technique across various compounds (charged or uncharged), cell types, phenotype alterations and organisms [64]. However, microinjection is a labor intensive technique which requires significant skill

and equipment. The current microinjection setups are limited in throughput and hinder performance and success rates as they cause fatigue in users over long periods of time. Additionally, microinjection results in point-source addition of molecules at a single site of interest. It can prove time consuming when delivery of multiple points is required.
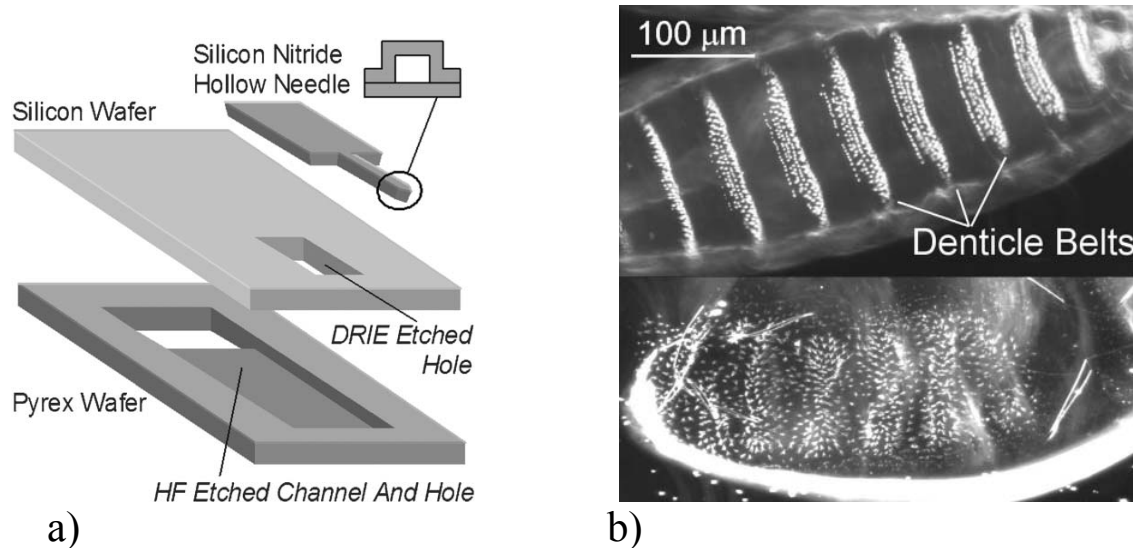
Figure 3.2: **An example of MEMS injection systems is presented. a) A simplified design of surface micromachined silicon nitride microinjector with integrated Pyrex glass channel reservoir. b) Top: cuticle of wildtype embryo with distinct denticle belts. Bottom: destroyed order of denticle belts due to microinjection of RNAi. Adapted from [67].**

3.2 MEMS injection systems

Aimed at replacing traditional microinjection needles, numerous MEMS-based injection systems have been developed over the past several years [64, 65, 66]. The advent of MEMS technology has enabled researchers to develop automated microinjection systems that offer cost-effectiveness and mass fabrication. Such systems are often accompanied by complete automation and high speed [64, 67]. In most MEMS injectors, a long hollow needle is fabricated by a sacrificial release process [68, 69]. A reservoir is built at one end of the needle which contains the desired compound and fills

the channel via capillary action. On applying an externally applied air pressure pulse, the liquid ejects out of the hollow needle from the other end. The injector geometry ensures repeatability of penetration and precise dosage of injections in most systems. These needles are often accompanied by computer-controlled robotic systems, which scan, locate and immobilize samples and perform precision injections [64, 67].

In the past, MEMS injection system applications have included transdermal liquid transfer [70, 71], controlled injection of DNA into cells [72] and drug delivery during neural recording with silicon probes [73]. Several of such injection systems can be operated in parallel so that one technician can conduct multiple experiments as compared to manual injection. However, automated systems are still based on permeating the membrane physically and dose the entire embryo or cell. Requirement of multiple points is still not met and most of these systems can be expensive and can not be utilized in typical biological laboratories.

3.3 Iontophoresis

Iontophoresis utilizes a small amount of electric current to push extracellular compounds inside a cell membrane. The compound is delivered in proportion to the current, which is readily adjustable. Briefly, a glass capillary acts as a chamber containing a solution of charged compounds (drug) to be delivered. An electrode is lowered into the capillary and immersed into the drug. When the same polarity charge (as on the drug) is applied to the electrode, it repels the charged drug molecules and drives them into the body [74, 75, 76, 77].

Iontophoresis has recently been used to introduce specific mRNAs into individual premigraotry neural crest cells to affect their differentiation and could be applied to many problems at late developmental stages of growing embryos [78]. Unlike some other techniques, iontophoresis is less dependent on biological variables such as membrane permeability and thickness. However, a number of other factors regulate iontophoretic transport such as current density, membrane pH and resistance, drug concentration, molecular size and time applied. Other common problems associated with iontophoresis include the effects of non-vasoactive compounds (vehicles for the active drug) such as DI water, tap water, sodium chloride solution etc., which increase membrane perfusion and are not the result of the drug being studied [79 - 83].

3.4 Electroporation

Electroporation refers to the use of strong local electric fields to transiently create pores and increase the permeability of a cell membrane to foreign compounds. With the added energy of a local electric field, the lipid bilayer of the membrane reorients itself to find the lowest energy state and in the process, creates short lived pores. While a pore is open, extracellular compounds can enter the cell. Successful electroporation of a cell is strongly dependent on various factors such as the amplitude, frequency, overall shape and no. of pulses of the applied potential and is usually empirically determined for each cell type. A range of these parameters exists wherein membrane pores reseal themselves after delivery [84]. Excessive field strength or long durations can cause irreversible damage to the cells [85].

Electroporation of DNA in mouse myeloma cells was first demonstrated by Neumann *et al.* [86]. Since then, electroporation has come into widespread use for gene, protein and

drug delivery into a variety of cell types [87, 88, 89, 90]. Current electroporation techniques require commercially built cuvettes and electroporators, and result in whole organism dosing as transient pores are created throughout the organism. With regards to zebrafish, electroporation is used in conjunction with microinjection to improve the delivery efficiency [91]. However, there is a growing need for patterned electroporation of compounds into developing embryos [92, 93] for further studies and such a need can be met by designing microfabricated electrodes on a glass substrate as demonstrated in Chapter V.
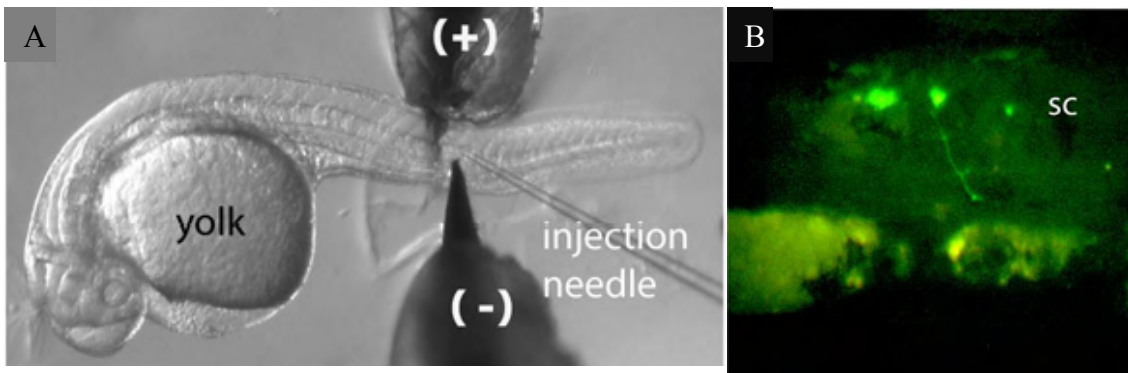
Figure 3.3: **An example of electroporation is presented. a) A biomolecule is first injected using microinjection and probes are simultaneously utilized to conduct electroporation and increase the efficiency of the delivery. b) A fluorescent signal confirms the delivery and integration of the biomolecule with the nucleus of the cell. Adapted from [91].**

3.5 Femtosecond Lasers

Recently, femtoseconds (fs) lasers have been utilized to noninvasively create transient pores and manipulate cellular material. These pores represent the absence of membrane material that has been removed by the laser (i.e. ablated). Laser ablation uses very short wavelength pulses at very high intensities to remove membrane or dielectric material from the surface of a material. It should be noted that these pores have no resemblance to

protein pores that are either hydrophobic or hydrophilic based on their internal amino acid compositions.

Konig *et al.* [94] reported the first use of fs laser pulses as a novel tool for dissecting chromosomes. Kohli *et al.* [95] have recently used lasers to introduce extracellular compounds in developing zebrafish embryos. The advantage of this technique lies in the high resolution that it offers. However, it remains a difficult technique to replicate in unspecialized biological laboratories.
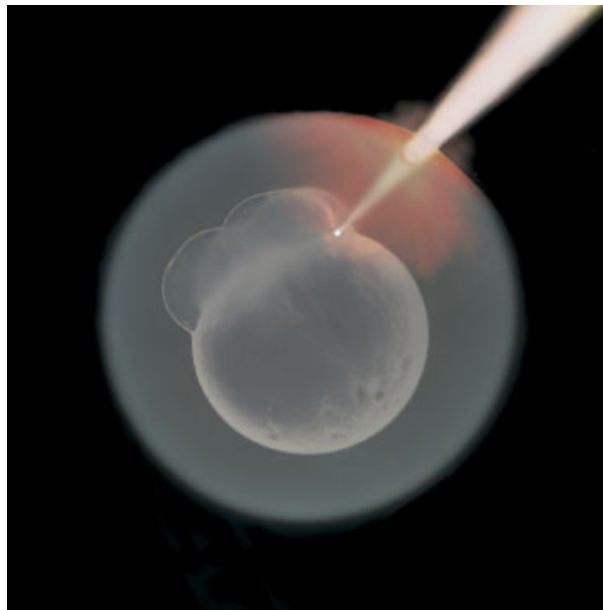
Figure 3.4: **When femtosecond (fs) laser pulses are focused through the chorion, laser induced transient pores are created at the blastomere-yolk interface or in individual blastomeres of zebrafish embryos. The pores are used to introduce foreign material into the embryonic cells. Adapted from [95].**

3.6 Other techniques

3.6.1 Photo-mediated gene activation

Photo-mediated gene activation technique utilizes a 'caging' process in which RNA is first inactivated by means of covalent attachment with a photo-removable protecting

group (the caging group), and later reactivating it by photo illumination with a specific wavelength [96]. To control gene expression in developing embryos such as zebrafish, it is essential to use a caging agent that easily reacts with mRNA *in vitro* and can be removed *in vivo* with a minimum amount of photo-illumination, thereby preventing excessive damage to embryonic tissues. Ando *et al.* [97] used a synthetic compound 6-bromo-4-diazomethyl-7-hydroxycoumarin (Bhc-diazo) which forms a covalent bond with the phosphate moiety of the sugar-phosphate backbone of RNA during caging. The 6-bromo-4-diazomethyl-7-hydroxycoumarin (Bhc) group binds to 30 sites on the phosphate moieties per 1kb of RNA sequence and undergoes photolysis (uncaging) when exposed to long wave ultraviolet light (350 – 365 nm).
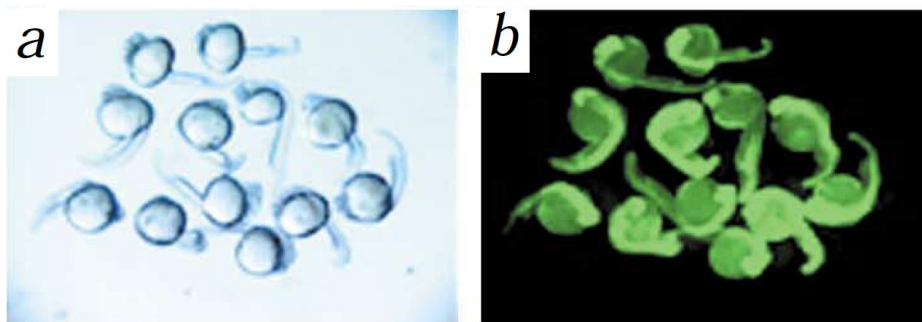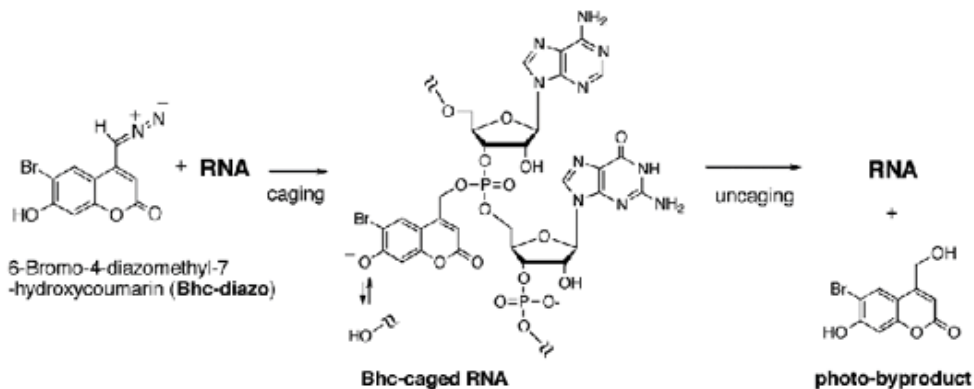
Figure 3.5: **Photo-mediated gene activation utilizes a 'caging' process where biomolecules are inactivated by a photo-removable protecting group and reactivated by illumination with a specific wavelength. Adapted from [97].**

3.6.2 Optoelectronic tweezers

Optoelectronic Tweezers (OET) technique utilizes light patterns to focus high-resolution electric fields on a photoconductive surface for manipulating cells. In optoelectronic tweezers, an incoherent light source (a light emitting diode or a halogen lamp) is reflected off from a digital micromirror display onto a photoconductive surface to generate patterns of conducting and non-conducting areas. A cell is placed on the conducting area and if the electric field is large enough, it causes electroporation which forms nanoscopic pores in the membrane, thereby allowing exogenous molecules to enter the cell [98, 99].
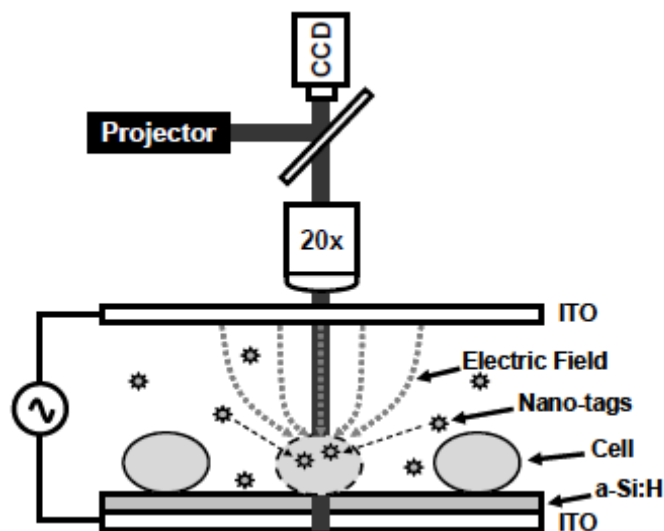
Figure 3.6:   **Overview of OptoElectronic Tweezer (OET) electroporation platform. Patterned light localizes electric field across a cell of interest resulting in selective electroporation and allowing extracellular compounds (e.g. molecules, nanoparticles) to enter the intracellular matrix. Adapted from [99].**

3.6.3 Aquaporins

Aquaporins are a type of intergral membrane proteins that are found in the cell membrane and are responsible for forming pores in the membrane. They are also known as water channels that selectively allow water molecules to in and out of a cell but

impede the transfer of other ions and solutes. Injection of aquaporins in zebrafish increases membrane permeability to water and cryoprotectants in the entire embryo[100].

3.7 Conclusion

There are a variety of techniques that exist to introduce extracellular compounds into growing embryos with each technique having its unique advantages and disadvantages. Most techniques utilize point-source delivery of extracellular compounds and dose the entire cell. Additionally, they are hard to replicate in biological laboratories. We developed a simple technique to deliver multiple compounds simultaneously as discussed in the next chapter.

CHAPTER IV

A MICROSYSTEM FOR DISTRIBUTED, TWO DIMENSIONAL CHEMICAL DOSING

The design, fabrication, characterization and results of a microsystem for distributed, two-dimensional dosing of chemicals into developing embryos is presented. The system consists of arrays of valved micropores which can be individually electrostatically gated to pattern gradients of diffusible molecules (as opposed to forced convection or other fluidic motion). The system's advantage lies in its simple valving scheme, which allows for the construction of high density microfluidic arrays of actuatable micropores for use with arbitrary molecules. Additionally, elastomer-metal devices are also constructed and their use as actuators and microfluidic valves is demonstrated. These devices carry the potential to be used *in vivo* due to their low power consumption and electrical actuation, and can be scaled down to operate at CMOS voltages.

4.1 Introduction

Traditionally, most microvalves are obtained using MEMS-based bulk or surface micromachining technologies which have been well established in the MEMS field during the last two decades [101, 102, 103, 104]. Electrostatic actuators are categorized as *mechanically active* microvalves where mechanically movable membranes are coupled to magnetic, electric, piezoelectric or thermal actuation methods. Sato *et al.* were the first

to report an electrostatically actuated gas microvalve [102]. Most electrostatic microvalves reported since then have been used to regulate gas flow only due to electrolysis problem associated with liquids under high voltages [105, 106]. Recently, a family of elastomer-based (usually polydimethylsiloxane) devices and systems have become popular due to their simplicity of monolithic fabrication, low equipment costs and ready compatibility with existing life science lab equipment (i.e. they are actuated with laboratory pumps and valves as opposed to electrical equipment) [107–109]. Some of these devices, however, depend on pneumatically-actuated pumps and valves which require two-layer PDMS processes and many pressurized external gas lines (40– 100 kPa) to operate, even when employing a variety of clever multiplexing techniques [109, 110, 111]. Moreover, the material suffers from a serious drawback in that it swells in most organic solvents. The swelling of PDMS-based devices makes it impossible for organic solvents to flow inside the microchannels. The dependence on external pneumatic actuation is also becoming increasingly problematic with the push towards integrated, high-density microfluidic systems which require thousands of independent valves [112]. Additionally, the lack of low power actuation schemes has, in part, prevented the adoption of these polymer devices for use in vivo [113].

Here we present an array of 'wet' MEMS actuators for use in cell and embryo culture. These actuators are based on gated micropores which actuate due to electrostatic pull-in with high frequency sinusoidal voltages. A 5 x 5 array of independent valves was designed, fabricated and tested. Actuation of the valves occurred at 23 V at 5 MHz sine wave signal and was confirmed both optically and by a non-contact profilometer. Actuation was carried out in air, oil and water medium. A 2 pore open-closed-open cycle

32

is demonstrated through electrostatic actuation which can be extended into multiple pores. Electrolysis in the device was averted by preventing the build up of electric double layer charge by using high frequency signal [115, 116].

Additionally, a class of 'wet' MEMS elastomer-metal electrostatic actuators which can actuate in air, organic solvents or water environments with no external fluidic connections is also reported. These actuators were termed as 'elastomer–metal' electrostatic actuators because they utilize a thin metal for electrical connection and an elastomer material as a movable diaphragm during electrostatic actuation pull-in when presented with a high frequency sine wave signal. These valves can be readily integrated into existing single-level PDMS microfluidic systems, can be actuated with no external valving and require low temperature processes. These valves can be grouped together to form classic peristaltic valves [114] and pumps, or combined with pores to build low power, programmable drug dosing elements. Conceptually, these devices are scalable into nanofluidic regimes and are compatible with CMOS processes.

4.2 Device theory and concepts

4.2.1 Pull-in Voltage

Electrostatic actuation is a well known process in 'dry' MEMS. On applying a potential between two parallel plates, electrostatic forces pull both the plates together. If the plates are held apart by a linear spring, the maximum range of travel is limited to 1/3 of the original gap after which electrostatic force exceeds the spring force and the gap collapses (assuming the potential is held constant). This 'pull-in' voltage is given as [115, 119]:

33

$$V_{PI} = \sqrt{\frac{8k(g + (t_{ox}.\varepsilon_{rL})/\varepsilon_{ox})^3}{27\varepsilon_0 \varepsilon_{rL} A_{cap}}}$$
(4.1)
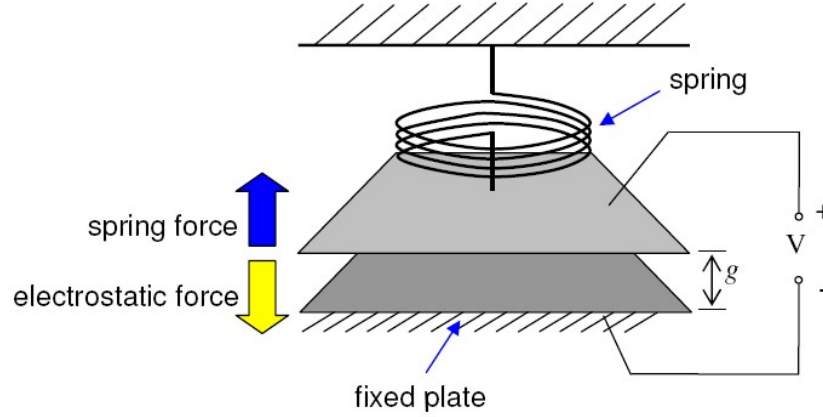
Figure 4.1: **Basic model of an electrostatic actuator. The top plate is mobile as compared to the bottom plate which is fixed. On applying a potential between two plates, electrostatic forces develop which counteract the opposite spring force and pull both the plates together.**

where k is the mechanical spring constant of the spring holding the plates apart, g is the initial distance between the plates, t_{ox} is the thickness of any solid insulating layer covering the plates, ε_{ox} is the relative permittivity of the solid insulating layer, ε_{rL} is the relative permittivity of the material between the plates (e.g. air, water, oil; this is the content of the fluidic channel), A_{cap} is the area of overlap between the capacitive plates, and ε_0 is the permittivity of free space (An explanation on how Equation 4.1 is derived is provided in Appendix A). Even though filling the space between the plates with water ($\varepsilon_{rL} = 80$) would provide very low pull-in voltages, operation in water has historically been limited due to the problems related with electrolysis [116], anodization [116] and electrode polarization [117]. This, of course, does not occur in oil filled plates and DC voltages are sufficient to close the plates. In order to operate in water, a high frequency

AC drive wave with no DC bias is necessary to prevent double layer screening of the electrostatic forces [118]. Note that as water has such a high dielectric constant, the thickness of any passivating dielectric cannot be ignored in the pull-in voltage calculations (Eqn. (4.1)) [119]. The devices presented here use this phenomenon to collapse the 'roof' of a conventional metal or PDMS microchannel onto the 'floor'. This collapse can be used as a valve in the same way that 'Quake' valves use pressure to collapse a PDMS roof and seal a microchannel.

4.2.2 Spring constant *k* for a rectangular plate

The spring constant is a good measure of the 'stiffness' or strength' of a spring. Most springs obey Hook's law of elasticity where the restoring force exerted by a spring is directly proportional to the spring constant and the distance the spring has been stretched:

$$F = -kx \tag{4.2}$$

where F is the restoring force of the spring, k is the spring constant and x is the distance the spring has moved.

For a rectangular plate, k depends on several parameters such as types of loading (point or distributed loading, in-plane or anti-plane, moment or torque), plate dimensions (lengths and thickness), material properties, and boundary conditions (fixed or simply supported). For a rectangular linear elastic plate with either fixed or simply supported boundaries, the spring constant can be calculated using closed form equations. In a square plate under anti-plane distributed loading, the spring constant k is expressed as [116]:

$$k = \frac{E \cdot t^3}{\alpha \cdot b^2} \tag{4.3}$$

where E is the Young's modulus of the plate, t is the plate thickness, b is the edge length, and α is a boundary condition coefficient. Boundary coefficients for different ratios of plate length and width are provided in [120]. For all simply supported edges, $\alpha = 0.444$; for all fixed edges, $\alpha = 0.0138$. Substituting equation (4.3) into (4.1) yields:

$$V_{PI} = \sqrt{\frac{8Et^3\left(g + t_{ox}\varepsilon_L / \varepsilon_{ox}\right)}{27\alpha \cdot b^2 \varepsilon_0 \varepsilon_L A}} \tag{4.4}$$

4.2.3 Electric Double Layer

Electric double layer (EDL) is a model which describes the interaction of electrode surface charges with electrolytic solutions. The model, first proposed by Helmholtz [wiki reference] in 1879, assumes the electrode to hold a charge density which arises from either an excess or deficiency of electrons at the electrode surfaces. In order for the interface to remain neutral, the surface charge is balanced by the redistribution of ions close to the electrode surface. These attracted approach the electrode surface and form a layer balancing the electrode charge. The overall result is two layers of charge (the double layer) and a potential drop which is confined to only a small distance from the electrode surface (Figure 4.2). The model is analogous to an electrical capacitor which has two plates of charge separated by some distance and eventually results in reducing or eliminating the applied force and actuator displacement [119]. If the electrode charge is completely screened by a diffused double layer, the actuator gets disabled. Since most electrostatic MEMS actuators typically require at least 1 V to operate, charge screening is important even in a high dielectric medium such as water.

EDL formation can be prevented by driving the actuator with an AC square wave of sufficiently high frequency, so that the ions do not have sufficient time to accumulate at the electrodes. In this case, electric field appears uniform, and since the electrostatic force is independent of the polarity of the applied potential, the actuator can be displaced as in
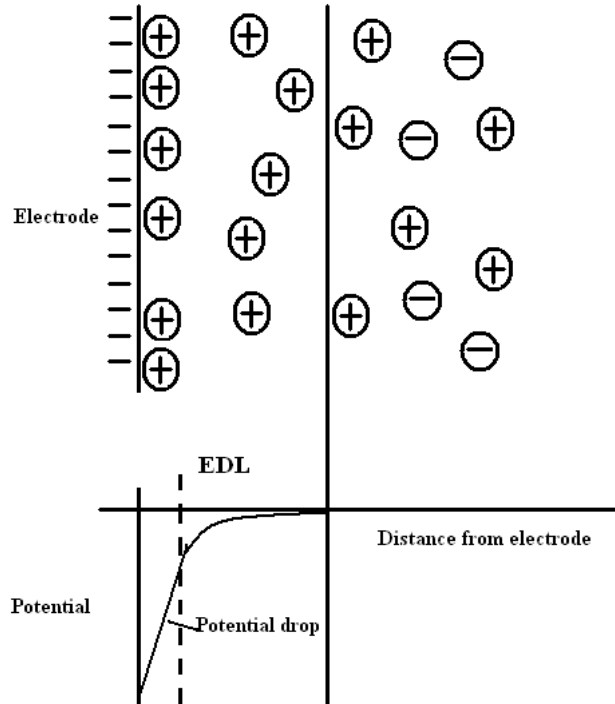
Figure 4.2: **Schematic of Electric Double Layer (EDL). EDL charge formation results in higher applied potential. It can be eliminated by driving the actuator with an AC square wave of sufficiently high frequency.**

an ideal dielectric [18, 19]. The frequency transition from a completely screened potential to a uniform electric field occurs when the time given for the ions to migrate in one direction is on the order of the time scale for screening the electrode charge. Double layer formation was prevented in our devices by using radio frequency (RF) in the range of 5 – 10 MHz.

4.2.4 Device concept

As a potential is applied between the top and the bottom electrode, electrostatic actuation is utilized to collapse the top membrane onto the floor to close the channel gap. This collapse is used the same way that 'Quake' valves use off-chip pneumatic pressure lines to collapse a PDMS membrane and seal a micro channel. Essentially by using electrostatic pull-in as the actuation mechanism the device is a self-actuating 'Quake' valve. This purely electrically-controlled approach also avoids external pneumatic connections. Table 4.1 summarizes all the values that were utilized to create the device and optimize the pull-in voltage (the most critical parameter) to within 15 V and 25 V for the elastomer-metal and all-metal device respectively.

Device configuration	Elastomer-metal	All metal (gold)
Membrane length	600 μm	600 μm
Membrane thickness	16 μm	2 μm
Channel height gap	8 μm	5 μm
Oxide permittivity	3.9	3.9
Oxide thickness	0.45 μm	0.45 μm
Liquid permittivity (water)	78	78
Membrane Young's modulus	160 MPa [21]	78 GPa
Membrane residual stress	2.6 MPa [21]	40.1 MPa [22]
Membrane Poisson's ratio	~ 0.5	0.42
Designed Spring Constant	6.76 N/m	26.36 N/m
Calculated Pull-in Voltage	6.29 V	9.79 V

Table 4.1:   Device design parameters are summarized. Designing devices with lower pull-in voltages led to flimsy devices that collapsed due to stiction.

4.3 Device fabrication

Two types of devices were explored. In the first, an all-metal microchannel was patterned over oxide-insulated indium tin oxide (ITO) electrodes using resist as the microchannel mold (Fig. 4.3a). The roof served as one capacitive plate and the ITO electrode formed the other. In the second design, the channel was made from PDMS instead of gold, but a thin gold layer was patterned into a compliant electrode within (or below) the PDMS. Spring constants (k) for the various roof designs were calculated using the well-known Roark's Formulas for Stress and Strain equations for either a rectangular mechanical plate with four fixed boundaries (page 462 of ref. 20) or using the equation for the appropriate flexure (e.g. spiral or meandering spring [120]) as mentioned above. Figure 4.3 shows the fabrication process. The devices were fabricated on 4" glass substrates. Transparent indium tin oxide (ITO) electrodes were sputtered (1500Å) and patterned through a liftoff process and annealed at 750 ºC in a Rapid Thermal Anneal (RTA) oven (Fig. 4.3a). A thin layer of oxide (0.45µm) was deposited via plasma-enhanced chemical vapor deposition (PECVD) and annealed in a RTA oven at 700 ºC (Fig. 4.3b). Contacts were timed etched through the oxide in 49% BHF (0.1µm min^{-1}) (Fig. 4.3c). A 5µm resist (Shipley 1827) for all-metal devices or a 10µm resist (AZ® 9260) for elastomer–metal devices was spun and patterned into desired microchannel geometries (Fig. 4.3d). Cr/Au (150Å /5000Å) was then evaporated onto the chip to form the top electrode (Fig. 4.3e). For elastomer–metal devices electroplating was not needed (Fig. 4.3f) and the gold flexures were patterned via wet etching (Fig. 4.3g). The patterned resist was flood exposed, developed and a new resist was spun on the wafer. The wafer was then diced. The resist was flood exposed once again and developed. Cr was removed

from individual dies with standard Cr etchant. 16µm of Dow-Corning WL-5150 photopatternable PDMS was then spun on. The sacrificial channel photoresist was then removed by immersing the chip overnight in acetone. Standard critical point drying (CPD) was performed to release devices (Fig. 4.3h2). Contact pads were wire-bonded to a carrier PCB board and soldered.
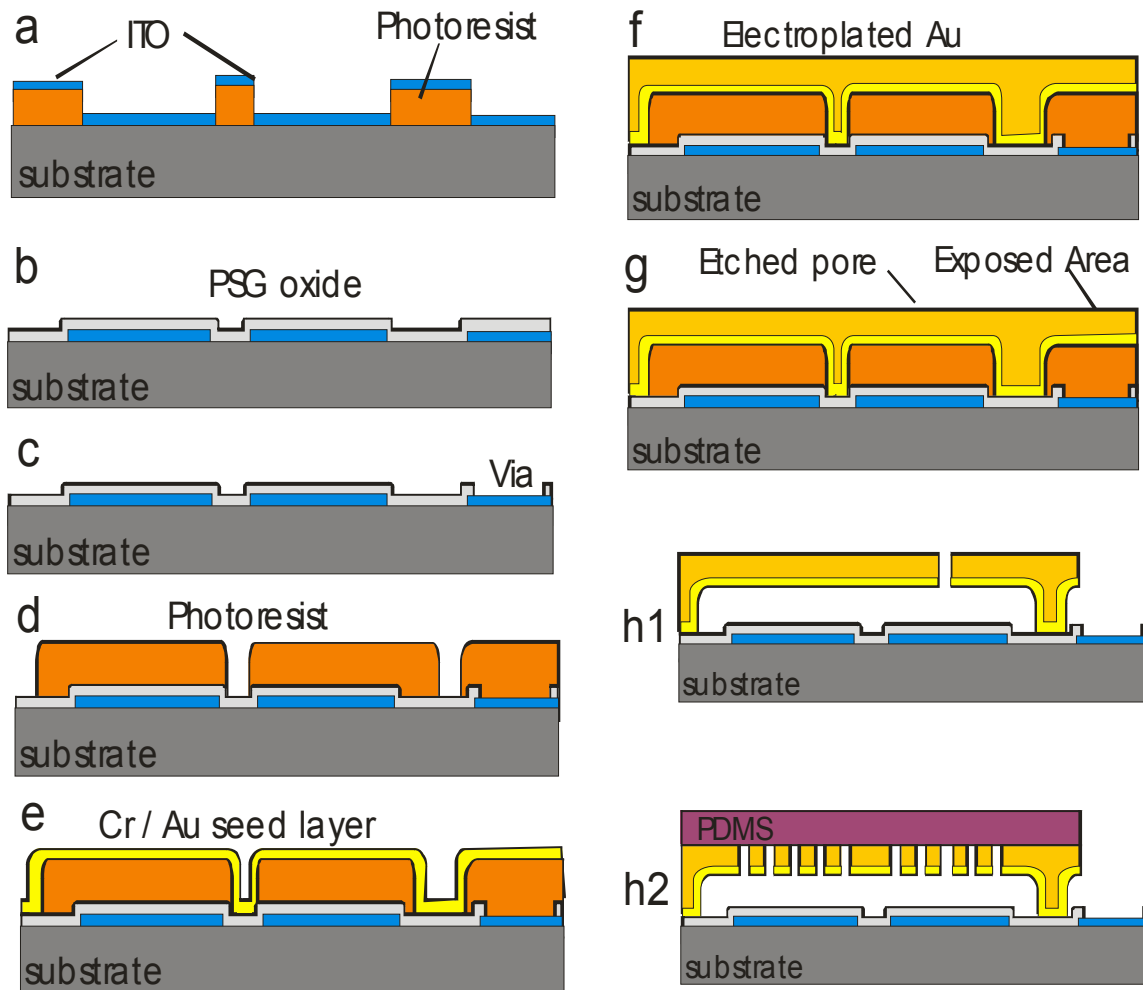
Figure 4.3: **Fabrication process flow for wet electrostatic actuators. Two types of devices were fabricated. h1) The all-metal devices had gold roofs which were selectively etched to create micropores. h2) The elastomer-metal devices had PDMS roofs and a thin layer of gold as electrical connects.**

40

4.4 Experimental setup

4.4.1 Dye preparation

For fluorescent imaging and dosing, a mixture of de-ionized water and a Tris(2,2'-bipyridyl)dichlororuthenium(II) hexahydrate (Sigma) fluorophore was loaded in a reservoir and entered the microchannels through capillary action. Devices were also filled and actuated with silicone oil (data not shown).

4.4.2 Instrumentation and microscopy

Upright and inverted microscopy was done with a ZEISS Axioskop and a Nikon TE2000, respectively. Surface profilometry was carried out using a Zygo New View 5000. DC voltages were applied using a Keithley 2400 Sourcemeter. AC voltages were applied with Agilent 33250A Function/Arbitrary Waveform Generator, 80 MHz.

4.4.3 Agar preparation

A solution of Bacteriological agar (A5306 from Sigma-Aldrich) was prepared with a concentration of 14 gram/Liter. The solution was heated at 50 ºC for 2 minutes on a hot plate. The hot solution was poured in a Petri-dish and allowed to cool down at room temperature for 10 minutes. Once the agar cooled down, it solidified into a gel. The agar served as a hydrophilic medium into which fluorophore was dosed to obtain profiles.

4.5 All-metal devices

Figure 4.4a shows a fabricated all-metal device. To operate the device, ruthenium was introduced at the inlet and filled the microchannels with capillary action. The advancing

liquid phase pushed all of the gas phase out through the etched pores and formed a long column inside the microchannels. The actuation chambers (600 µm x 600 µm) inside the chambers were supported by the design of 50 µm x 50 µm posts to prevent membrane collapse during the release method due to stiction forces. To demonstrate diffusion from the micropores, a thin sheet of Agar (1 mm thick) was placed on the pores as shown in Figure 4.4b. As time elapsed, the intensity of the fluorophore decreased, while the gradient expanded radially (data not shown).
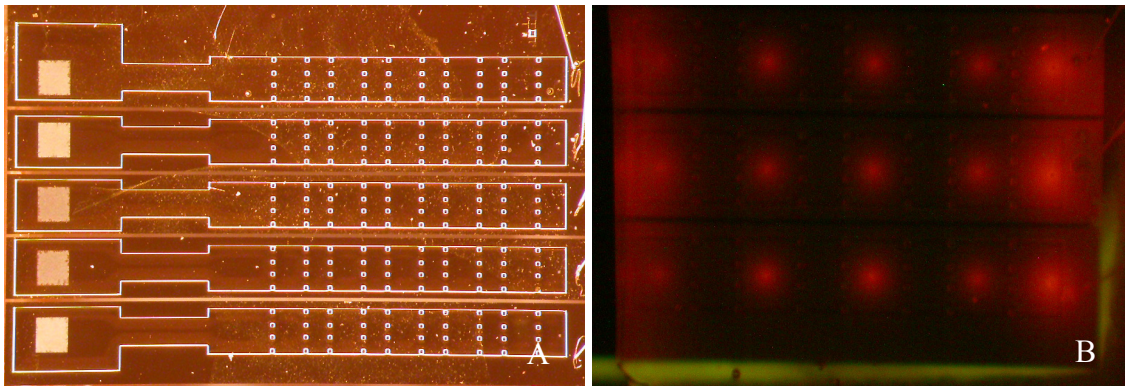
Figure 4.4:   **a) An all-gold fabricated device is shown. b) Diffusion occurs in normally open pores as ruthenium is introduced at the inlet.**

4.5.1 Pull-in characterization

The pull-in voltage for all-metal devices was characterized in both air and water as shown in Figure 4.5. The pull-in voltage for water ($\varepsilon = 80$) was 13 V as compared to air ($\varepsilon = 1$) which had a pull in voltage of 55 V. However, in both these cases, the pull-in voltage was much higher than elastomer-metal devices (this will be discussed in later sections).

4.5.2 Deflection characterization

Figure 4.6 shows an inverted optical and an inverted fluorescent micrograph, of an all-metal device. On applying a potential between the top metal electrode (ground) and bottom ITO electrodes, the device actuated and closed. Fig. 4.6c shows the same device under actuation at 18 V. Figure 4.6d shows the deflection profiles unactuated and profilometer.
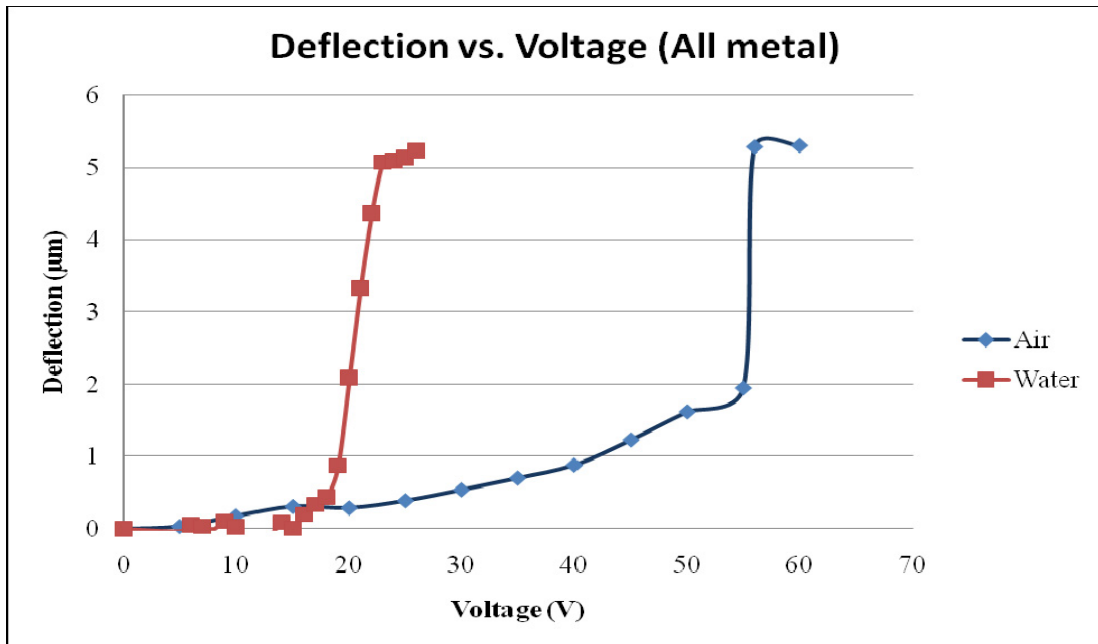
Figure 4.5: Deflection vs. voltage is characterized for all metal devices. Pull-in voltage for water and air was 23 V and 55 V respectively.

4.5.3 Power consumption

Gold has a maximum yield strength of 120 MPa; above that stress, metal devices would plastically deform and fail. It was thus important to ensure that the actuating stress did not deform the devices permanently. However, attempting to lower the pull-in voltage below 15V resulted in devices that were so flimsy that Laplace–Young pressure collapsed the channel during conventional release. Given a spring constant k, an overall gap of g

(4.95µm) and a final remaining gap of t_{ox} (0.45µm) after pull-in, the energy expended to close an actuator is:

$$E = \tfrac{1}{2}\, k*(g - t_{ox})^2 \qquad\qquad (4.5)$$
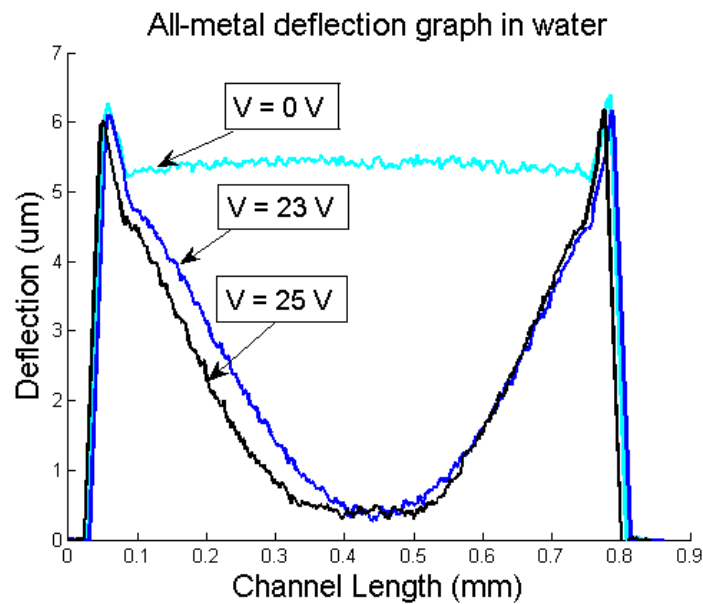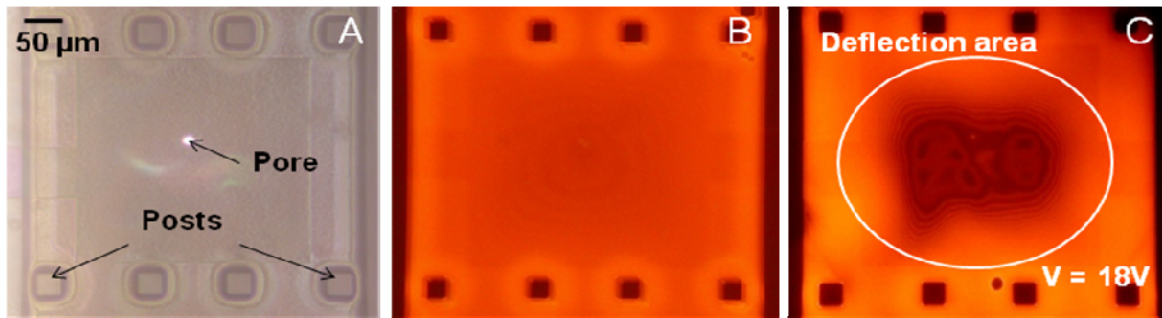
Figure 4.6: Visual and quantitative analysis of all-gold device deflection. a) All gold devices after release. b) One of many chambers in an all gold device filled with DI water and fluorescent compound. c) An actuated all gold device. d) Profilometry cross section confirming pull-in. Valve profiles completely flatten against bottom electrode above 30 V.

For the devices presented here, this corresponds to energies ranging from 0.55nJ to 0.67nJ. Peak currents were limited to 1 mA. All-metal devices closed within 1 s. Using

Equation 4.5 and the definition of power (P = dE/dt = E/t), this corresponds to an average power consumption of 110 pW.

4.5.4 Programming gradients

Figure 4.7 demonstrates how pixel-style programmable gradients can be achieved with all-metal devices. A fluorescent solution was filled in the microchannels and allowed to diffuse through the open pores. In the 'normally open' initial condition, the dye molecules diffused out from the pore into agar (hydrophilic medium, see above). After 30
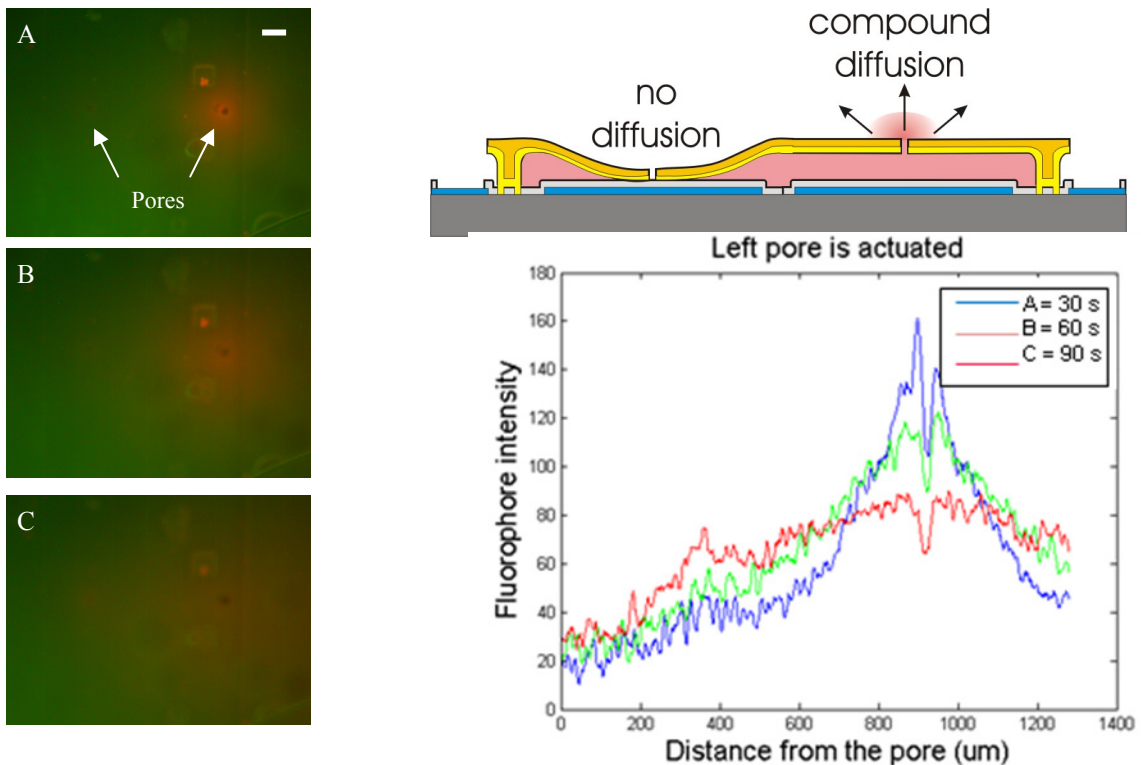
Figure 4.7a: **Left pore is electrostatically actuated and closed by applying a 25 V, 5 MHz potential between ITO electrode and metal roof, halting diffusion. Agar was replaced. Scale bar is 40 μm.**

sec, the left pore was electrostatically closed by applying a 25V, 5MHz sine wave signal which halted diffusion. The right pore remains unactuated and continued diffusion. As

more time elapsed, the concentration gradient expanded radially due to Fickian diffusion of the molecules and the intensity of the fluorophore declined. After 90 seconds, this signal was removed from the left pore and applied to the right pore, thereby closing it. A sequence of signals can be thus provided between different micropore chambers and programmed to obtain pixel style gradient profiles.
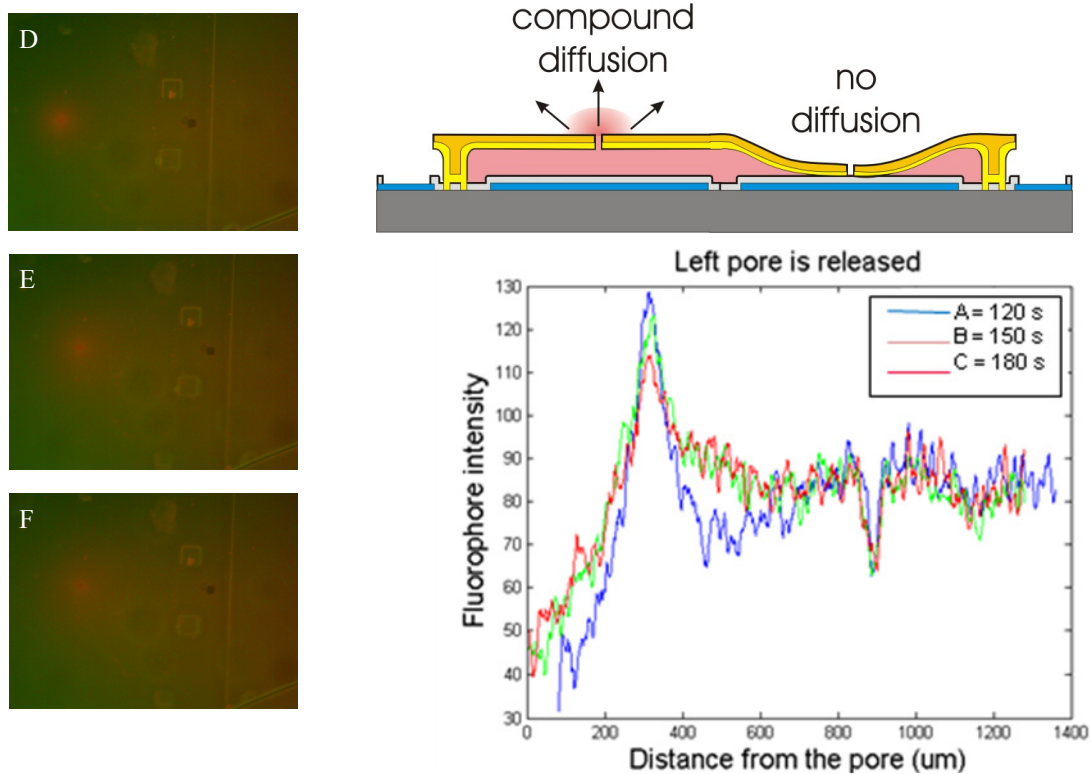
Figure 4.7b: **Left pore is released after actuation (V = 0 V between ITO electrode and gold roof). Right pore is electrostatically actuated and closed.**

4.6 Elastomer-metal devices

Elastomer-metal devices were fabricated to lower the pull in voltages observed in all-metal devices as shown in Figure 4.3h2. These actuators were termed as 'elastomer–metal' electrostatic actuators because they utilize a thin metal for electrical connection and an elastomer material as the main movable diaphragm during actuation when

46

presented with a high frequency sine wave signal. Elastomer materials have are less stiff than common metal, therefore have lower Young's modulus and spring constant (Equation 4.3) The advantage of these valves is that they can be readily integrated into existing single-level PDMS microfluidic systems, can be actuated with no external valving and require low temperature processes.

4.6.1 Pull-in characterization

Figure 4.8 presents the deflection voltage graph for elastomer-metal devices. The low Young's modulus of PDMS (160 MPa) [121], as compared to gold (78 GPa) resulted in a lower spring constant as described in Equation 4.3, thereby resulting in a lower pull-in voltage in both air and water environments (as compared to all-metal devices).
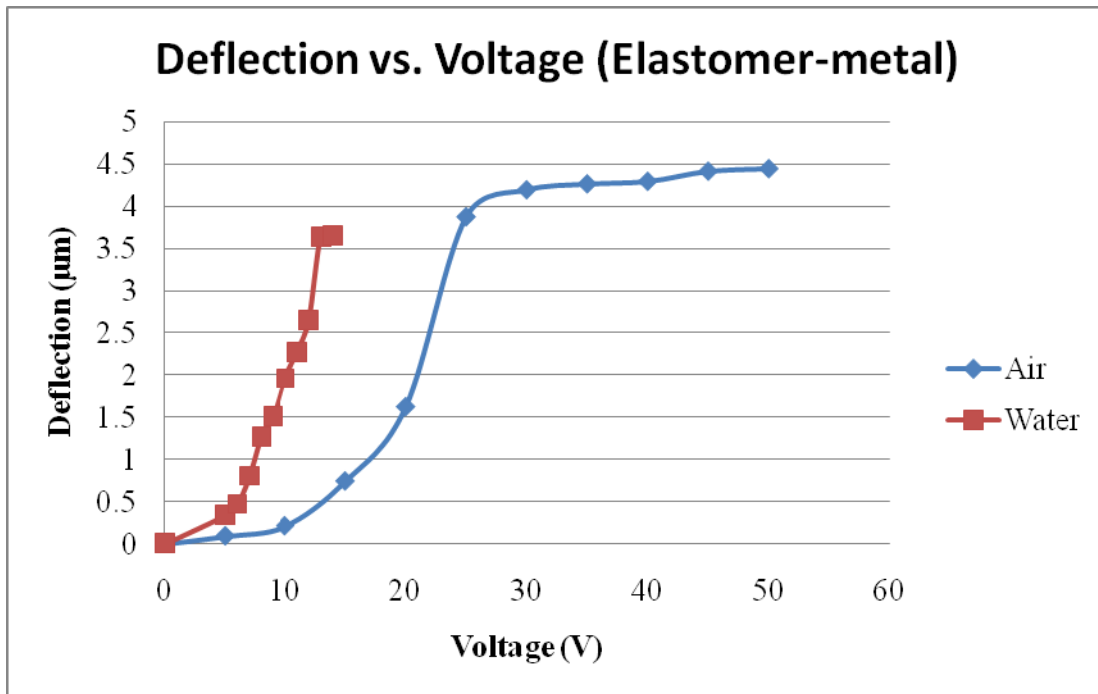
Figure 4.8: **Deflection vs. voltage graph for elastomer-metal devices. Pull-in voltage for water and air was 13 V and 25 V respectively.**

47

4.6.2. Deflection characterization

Figure 4.9 shows an inverted optical and an inverted fluorescent micrograph, of an elastomer-metal device. Like all-metal device, application of a potential between the top metal electrode (ground) and bottom ITO electrodes, the device actuates and closes. Fig. 4.9c shows the same device under actuation at 16 V. Figure 4.9d shows the deflection
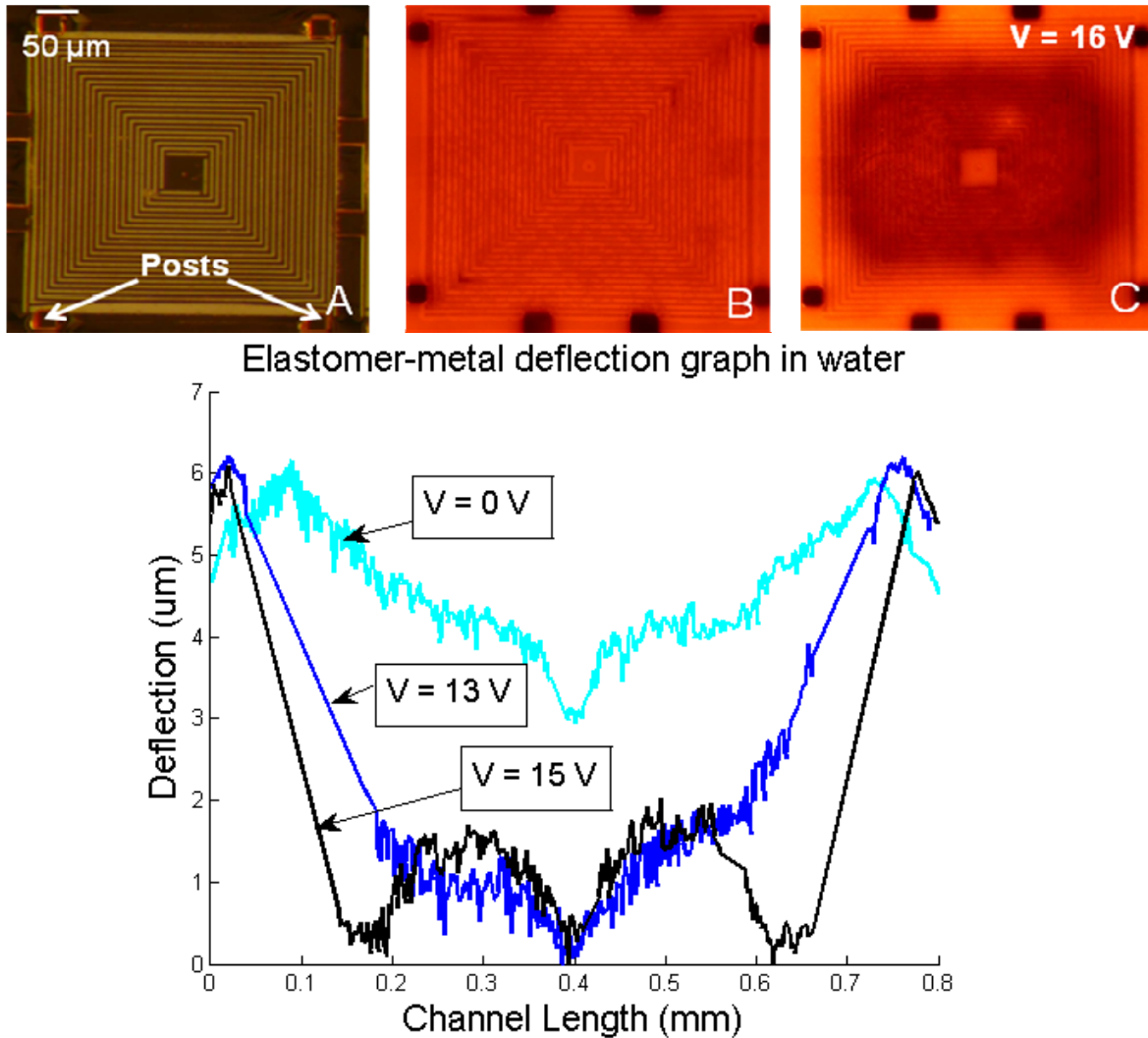
Figure 4.9: **Visual and quantitative analysis of elastomer-metal device deflection. a) Elastomer-metal just after release. b) One chamber filled with DI water and fluorescent compound. c) An actuated elsatomer-metal device. d) Profilometry cross section confirming pull-in. Better valve sealing is observed at higher voltages than pull-in voltages.**

profiles unactuated and actuated valves of all-metal devices obtained in water with the Zygo non-contact profilometer. Unlike all-metal device, the elastoer-metal devices sags a little because it is released in acetone which gets absorbed into the PDMS and results in volume dilation.

4.6.3 Power consumption

Using the definition of the energy expended to close the a spring elastomer-metal actuator as given in Equation 4.5, yields energies ranging from 0.19 nJ to 0.25 nJ. Elastomer-metal devices closed in 5 s which was slower than all metal devices due to membrane dilation and sagging of the elastomer. Given the definition of power (P = dE/dt = E/t), this corresponds to an average power consumption of 44.2 pW.

4.6.4 Valving operation

Fig. 4.10 demonstrates the operation of the device as a valve. For visualization purposes, fluorescent water mixed with microspheres (0.5 mm diameter) was used to fill a 6 mm microchannel. The liquid flow was observed by detecting the movement of the microspheres. Flow was established by evaporative pumping across the microchannel where an outlet pore was etched to push the gaseous phase out of the channel. Upon valve actuation, the membrane deflected down and microsphere movement stopped, the microspheres were expelled from between the electrodes, and piled up against the boundary of the ITO electrode as shown in Fig. 4.10b. Once unactuated, the valve opened and the microspheres continued their flow.
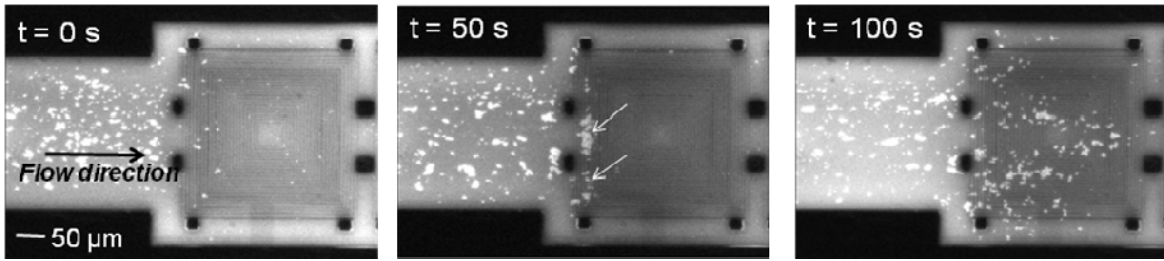
Figure 4.10: Elastomer–metal devices function as a microvalve. A) Microspheres (0.5 mm diameter) mixed with fluorescent solution were loaded into the microchannel. Beads flow under an unactuated valve. B) At t = 50 s the elastomer–metal valve was closed, stopping flow; microspheres were expelled by the valve and accumulated at the valve boundary, as pointed out by the arrows. This indicates that the flow was stopped. C) As the valve was opened at t = 100 s, the liquid flow resumed and the microspheres moved again.

4.7 Conclusion

The design, fabrication, characterization and results of a class of 'wet' MEMS actuators are presented. The actuators were designed to delivery pixel-style molecules into a developing tissue and are programmable. Additionally, elastomer-metal wet actuator movable diaphragms were also designed using a sacrificial microfabrication technology. Electrostatic actuation of the diaphragm was demonstrated in air and water environments at 13V and 25V respectively. A 3-phase valving sequence using AC voltages was also demonstrated. Typical chamber sizes were 600 μm wide, 600 μm long and 5 μm high. The actuators were designed using simple low temperature processes and can be grouped together to fabricate other microfluidic devices such as micropumps, peristaltic microvalves, ionization nozzles, and filters. We also present basic design theory as these devices are scalable into nanofluidic regimes conceptually and are compatible with CMOS processes.

CHAPTER V

PATTERNED DELIVERY AND EXPRESSION OF GENE CONSTRUCTS INTO ZEBRAFISH EMBRYOS

The design, fabrication and results of microfabricated interfaces for the patterned delivery of foreign molecules via electroporation into developing embryos is presented. These systems were used to 'draw' two-dimensional patterns of tracer molecules, DNA and mRNA into the yolk and cells of zebrafish embryos (*Danio rerio*) at different stages of development. The successful delivery of two-dimensional patterns of trypan blue (normal dye), texas red (fluorescent dye), pCS2eGFP DNA and GFP-mRNA in both chorionated and dechorionated embryos is also demonstrated. Both DNA and mRNA were expressed in the desired patterns subsequent to delivery.

5.1 Introduction

The ability to modify two dimensional specially-shaped areas with controlled delivery of genes and proteins in patterned shapes allows more biologically-relevant manipulations of a complete system's development [123]. Such control or 'hacking' tools are limited at this time and this technology provides a biological tool to study developmental mechanisms. Similarly, simultaneous delivery of multiple molecules in different patterns also expands the type of experiments performed in spatially

heterogeneous systems, particularly where multiple pathways with specific timings are involved [124, 125, 126].

In this work, 10 µm wide platinum electrodes were microfabricated into desired patterns and passivated with silicone elastomer. Square pulses of 10-20 V (0.20-0.40 kV/cm), 50-100 ms pulse width were sufficient to create transient pores and introduce compounds from the late blastula period (3 hpf) to early pharyngula period (24 hpf) embryos. Using 24 hpf dechorionated embryos, we achieved a high survival rate of 91.3% and 89%, and a delivery rate of 38% and 50% for GFP- DNA and GFP-mRNA respectively.

We believe that this simple technique offers the unique advantage of introducing foreign compounds at local sites and in specific patterns unlike any other microsystem technique and provides a new tool to aid advanced studies in cellular development and morphogenesis.

5.2 Theory of electroporation

5.2.1 Operation

During electroporation, transient pores are created in a cell membrane when short electrical pulses (exceeding the membrane's dielectric strength) are applied. While a pore is open, extracellular compounds in the vicinity of the pore can enter and transit into the cell interior. During conventional electroporation, a high concentration of cells and relevant molecules (dyes, proteins, genes, etc.) in suspension are introduced between two opposite electrodes. A high electric field, typically from 1-10 $kVcm^{-2}$, is applied to the electrodes to deliver the molecules into the cells [127, 128, 129]. Electroporation is a

well-characterized method for molecule delivery into embryos of many species [129, 130], although microinjection is more common for zebrafish embryos. As might be expected, compound trans-membrane permeability is highest for cells nearest to the electrodes [128]. The amplitude and frequency of the applied potential, as well as its overall shape and total duration are usually empirically determined for each cell type; a range exists wherein membrane pores reseal themselves after delivery [128]. Excessive field strength or long durations cause irreversible damage to the cells and the organism [129].

5.2.2 Field Induced Transmembrane Potential

The bilayer structure of a cell membrane is a dielectric. When a spherical cell in suspension is exposed to an electric field, the Maxwell equation describing the current in the region near the cell is given by:

$$\Delta \cdot J + \frac{\partial \rho}{\partial t} = 0 \tag{5.1}$$

Where J is the current density, ρ the resistivity, and t the time variable. If charges are not generated in a cell during electroporation treatment, this relation simplifies to:

$$\Delta \cdot J = 0 \tag{5.2}$$

Since the electric field is the gradient of electric potential, the Maxwell equation becomes:

$$\Delta^2 \psi = 0 \tag{5.3}$$

where ψ denotes the electric potential. If the conductivity of a cell membrane is much smaller than that of external medium, and the thickness of the low-conductivity shell is small compared to the outer radius of the sphere, the solution to the Maxwell relation for a field induced transmembrane potential, can be expressed as [131, 132, 133]:

$$\Delta\psi = 1.5 \, a \, E \, \cos\theta \qquad\qquad (5.4)$$

where a, E and θ are the outer radius of the cell, the applied field strength and the angle between the field line and the normal to the point of interest in the membrane. Equation 5.x has been shown to be generally applicable in most lipid vesicles [134, 135].

5.2.3 Circuit model of the cell and chip

The circuit model of this set-up is shown in Figure 5.1. The cell itself can be modelled as a parallel combination of a variable resistor and a capacitor (whose effect is transient). In parallel to the cell is the resistance of the medium R_{medium}. The potential drop across the cell is significantly greater than the drop in the medium. Moreover, since the phospholipid membrane of the cell has much higher resistance than both the cytosol and the extracellular medium, only the potential drop in the membrane is significant.
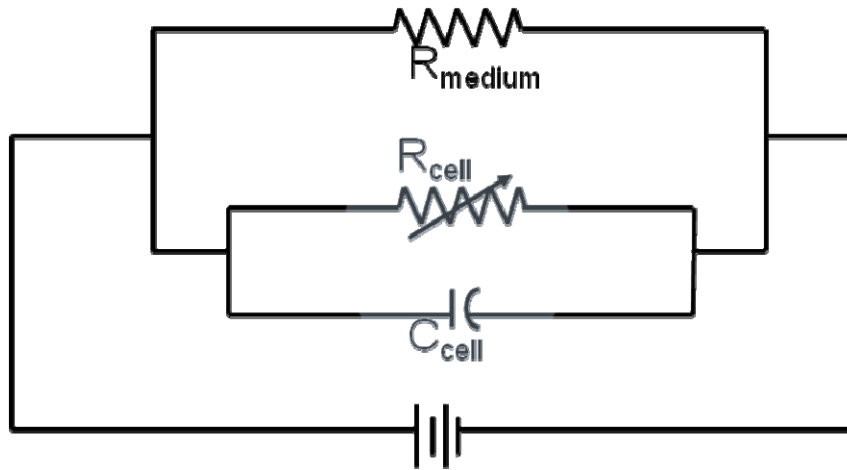
Figure 5.1: **The circuit model of the cell and the chip. The cell itself is modeled as a parallel combination of a resistive R_{cell} and a capacitive C_{cell} element. R_{medium} is the resistance of the medium and is parallel to Rcell as the current can by pass the cell through it. It is assumed that R_{medium} remains constant before and after electroporation. After electroporation the only element that changes in the model is the R_{cell}, which drops due to the formation of electropores.**

5.3 Device fabrication

All devices were fabricated on 4" glass substrates. Wafers were cleaned in Piranha (1:1 H_2SO_4:H_2O_2) for 20 minutes followed by a 10 minute rinse-dry cycle. Photoresist was then spun on, patterned into electrode geometries and soft-baked. A descum was
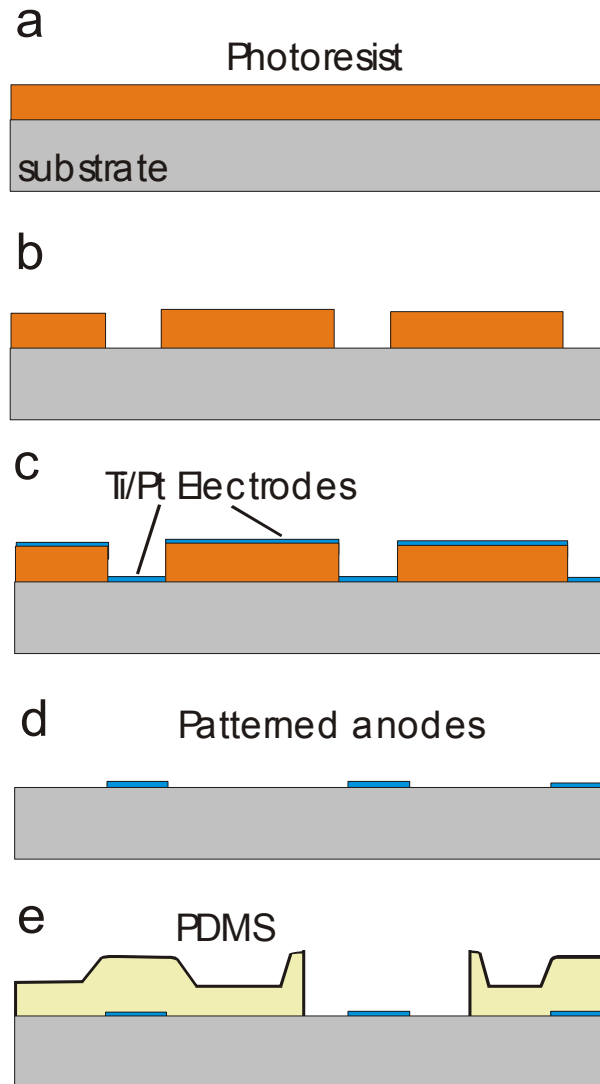
Figure 5.2: **Fabrication process. Liftoff process was utilized to fabricate patterned electrodes on a glass substrate.**

performed for 3 min at 80 W to remove any residual traces of photoresist; this enhances the lift-off yield significantly. Titanium (500 Å) and platinum (1000 Å) were deposited

using evaporation and patterned using a lift-off process. Parts of the metal areas were then passivated with Polydimethylsiloxane (PDMS) acting as the silicone elastomer, leaving only the relevant metal shapes exposed to electric fields. This passivation can be performed by either a) spinning and curing Sylgard® 184 and cutting out windows in the cured polymer using a sharp blade or b) spinning (300 rpm), baking (130 ºC, 2 min), lithographically exposing and curing (150 ºC, 2 min) Dow Corning® WL-5150 photo-patternable silicone (according to manufacturer's instructions) to pattern appropriate windows in the polymer. The resultant setup effectively shields electric fields and forms a chamber around the electrode to contain the solution (PDMS is hydrophobic) and the embryo.

A second set of multi-compound dosing devices were also constructed (See Appendix B). Metal microfluidic channels were fabricated over the electrodes via a sacrificial release method and micropores were wet etched in the channel roof. These devices could deliver multiple chemicals simultaneously into the embryo.

5.4 Experimental setup

5.4.1 Setup

Figure 5.3 illustrates the setup. During conventional electroporation in most organisms, electrodes are placed on both sides of the embryo and transient pores are created by providing electrical pulses between them. This creates pores in the entire organism. In zebrafish embryos, however, microinjection is first used to deliver extracellular compounds locally (Figure 4.1a) followed by electroporation of the entire embryo to enhance the microinjection results.

In this setup, lithographically-patterned metal (Figure 4.1b) on thin glass acted as the anode and a distant metal wire was placed in solution approximately 500 μm away and acted as the cathode (these roles were switched during negatively charged pCS2eGFP DNA electroporation delivery). PDMS was used both as an insulator and as a boundary around the anode to create a chamber and contain the movement of the embryo.
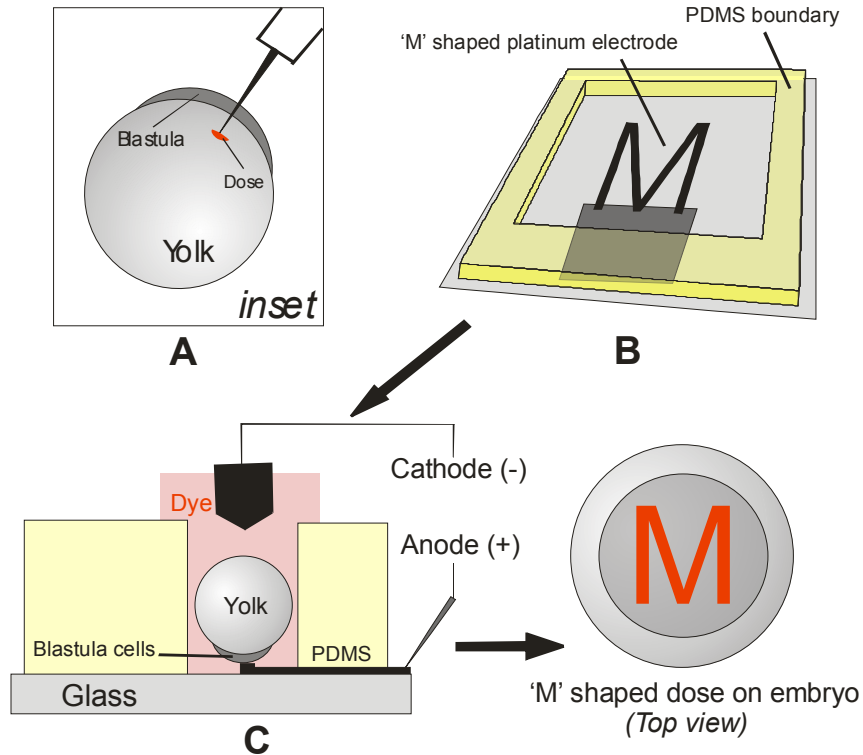
Figure 5.3: **Conceptual zebrafish electroporation setup is shown. a) Microinjection remains a common but labor intensive process. b) Microscale noble metal electrodes were fabricated on a glass substrate in our device. These electrodes acted as anodes during electroporation. c) During dosing, embryos were placed on top of the patterned anode. The PDMS boundary created a chamber which contained the dye solution. A second electrode on top of the embryo acted as cathode. On applying short electric pulses between electrodes (electroporation), electrode-shaped patterns of extracellular compounds were delivered into the embryo.**

During an experiment, the chamber was filled with embryo medium mixed with the appropriate delivery molecule. In the case of multi-compound dosing devices, the

microfluidic channels were first filled with the appropriate dyes (and no compound was introduced into the bulk medium). Embryos were then pipetted into the chamber where they settled on top the electrode.

The cathode was lowered on top of the embryo at this time. A commercial voltage source (Agilent 33220A) was used to deliver square wave pulses of 10-20 V, 50-100 ms pulse width between the electrodes. After the pulse was applied and electroporation conducted, embryos were gently removed from the device with a pipette and moved into a petri dish containing E3 medium and incubated in 28.5 ºC for 24 hrs.

5.4.2 Zebrafish rearing and preparation

Zebrafish embryos from the Duan lab were grown according to the procedure in [9], maintained on a 14 hr-10 hr light dark cycle. A stock solution of E3 medium was prepared (5 mM NaCl, 0.17 mM KCl, 0.33 mM $CaCl_2$, 0.33 mM $MgSO_4$, and 0.1% Methylene Blue) and once embryos were obtained subsequent to mating (usually daily), they were transferred in this medium and incubated at 28.5 °C. Embryos were de-chorionated by mixing in 125 µg/ml of Pronase (Roche) in E3 medium and gently shaking the petri-dish until the chorion came apart. They were rinsed thrice to remove all the pronase. Just before electroporation, embryos were anaesthetized by using MS222 (Sigma). During electroporation, embryos were held immobile within the PDMS wall chamber. They were gently pippetted into that chamber and positioned in the proper orientation over the stimulating electrodes using 5A tweezers and gentle pushing or using rolling motions. Methyl cellulose (Sigma) was also tested to hold embryos immobile, but

slowed throughput and did not provide a significant advantage toward proper positioning of the embryo with respect to the electrodes.

5.4.3 Dye preparation

For fluorescent imaging and dosing, solutions were prepared by mixing E3 medium with appropriate dyes. These dyes were chosen due to their low molecular weight. 30 mM solutions of Texas Red® Dextran 3000 MW, lysine fixable (Invitrogen) and Fluorescein were prepared. A 0.4% (by volume) trypan blue (GIBCO) solution was also prepared.

5.4.4 DNA and mRNA preparation

pCS2eGFP vectors were prepared according to the procedure outlined by Dave Turner and Ralph Rupp [10, 11]. Briefly, A DNA fragment containing the Kozak sequence followed by entire ORF of EGFP (Clontech, USA) was generated by PCR. This DNA fragment was subcloned into the pCS2+ vector to generate the EGFP overexpression plasmid DNA (pCS2+EGFP). The purified plasmid was dissolved in DNase free water and stored at -20 ℃ until use. The pCS2+EGFP plasmid was linearized by restriction enzyme (NotI) digestion and was used for capped EGFP mRNA synthesis. Capped RNA was synthesized by in vitro mRNA transcription using mMassage mMachine kit (Ambion, TX). Prepared EGFP mRNA was dissolved in diethylpyrocarbonate (Sigma, USA) treated water and kept at -80 ℃ until use.

5.4.5 Instrumentation and Microscopy

DNA-GFP imaging was done by Leica MZ 16F upright microscope. Adobe Photoshop and ImageJ were used to process figures. Upright and inverted microscopy was done with ZEISS Axioshop and a Nikon TE2000, respectively for dye imaging. Electroporation potential was applied with an Agilent 33220A Function/Arbitrary Waveform Generator, 20 MHz. Single square wave pulses of 10-20 V, 50-100 ms pulse width was applied between the electrodes.

5.5 Results and discussion

As with any electroporation protocol, long duration and high voltage pulses can kill cells [136, 137, 138]. The ideal voltage, pulse length and number of pulses is difficult to determine and changes for each setup. Here, we first determined these values experimentally (data not shown) by attempting a range of known good values [136] with a simple, straight electrode. These parameters (see below) were then used throughout the experiment.

5.5.1 Dye delivery

As a benchmark of basic electroporation, Trypan blue dye was electroporated in early stage (3-5 hpf) embryos with intact chorion. Two square pulse of 20 V, 100 ms pulse width, 1s apart were used. Electroporation created temporary pores in the chorion which enabled trypan blue to readily diffuse into the perivitelline space of the embryos as shown in Figure 5.4. To reduce the adhesion effect of trypan blue, the embryos were kept in E3

solution for 3 hrs before being imaged [136]. Control embryos (V=0) were used as reference.
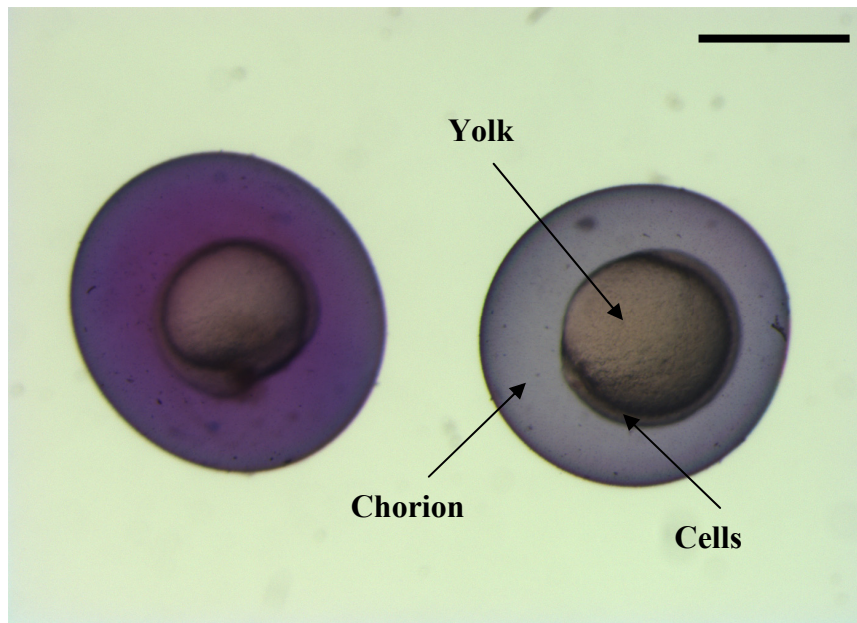
Figure 5.4:   **Successful delivery of trypan blue dye through the chorion of the embryo. Electroporation created temporary pores and trypan blue diffused inside the perivitelline space of the embryo (left). Electroporated embryos appeared deeper blue as compared to embryos with no electroporation (right). Scale bar is 300 μm.**

Next we used the devices to dose patterns of a fluorescent tracer dye (Texas Red) commonly used when tracking cell fate in embryos. Figure 5.5a shows a 10 hpf zebrafish embryo on top of a single, long 10μm wide fabricated platinum anode. Most of the electrode is covered with an elastomer. The embryo was aligned such that the yolk was in direct contact with the anode while the cathode was 500μm away. Two square pulses of 10V, 50ms pulse width, 1s apart were used. Figure 5.5b shows the fluorescent image of the embryo with the pattern of a point delivered in the yolk. Fig 5.5 c,d show a pattern of a line. Cells closer to the electrode tended to have sharper features. Only part of the line was imprinted onto the embryo due to the curvature of the yolk.
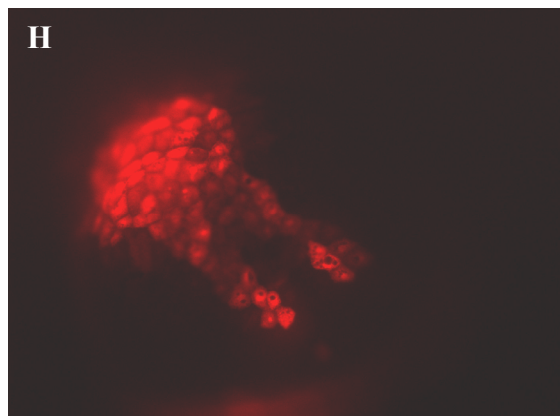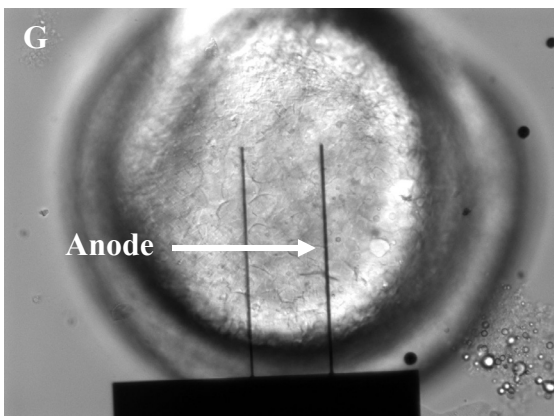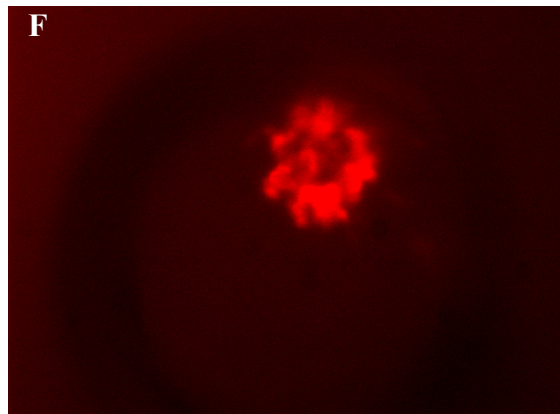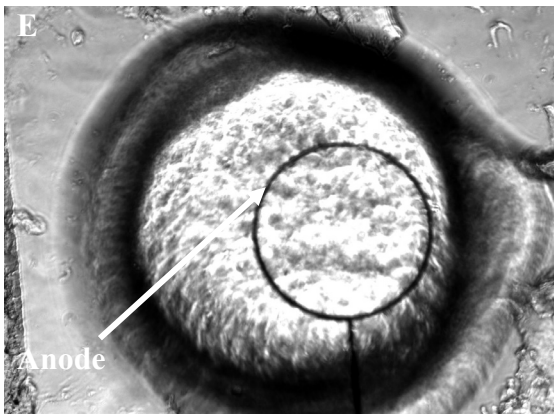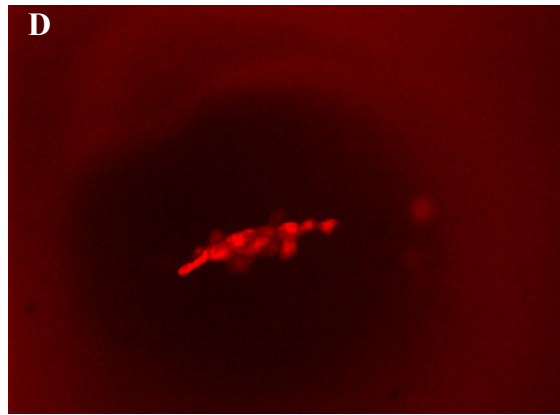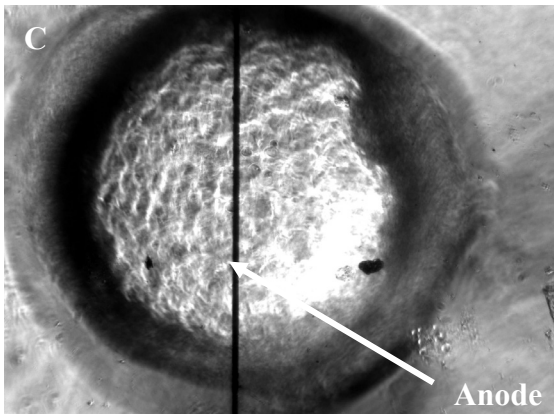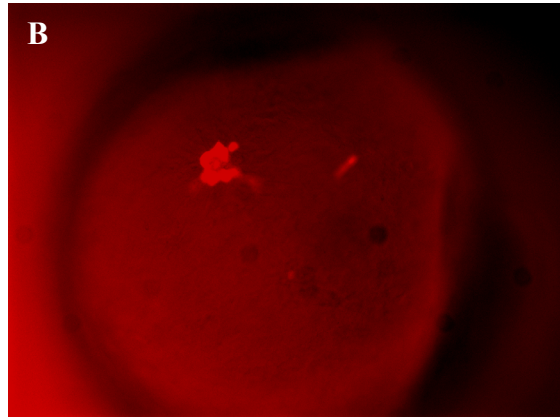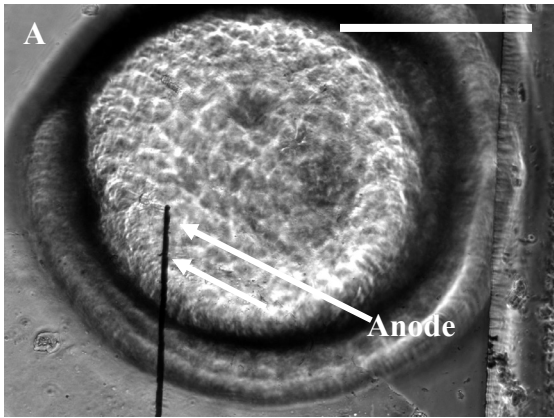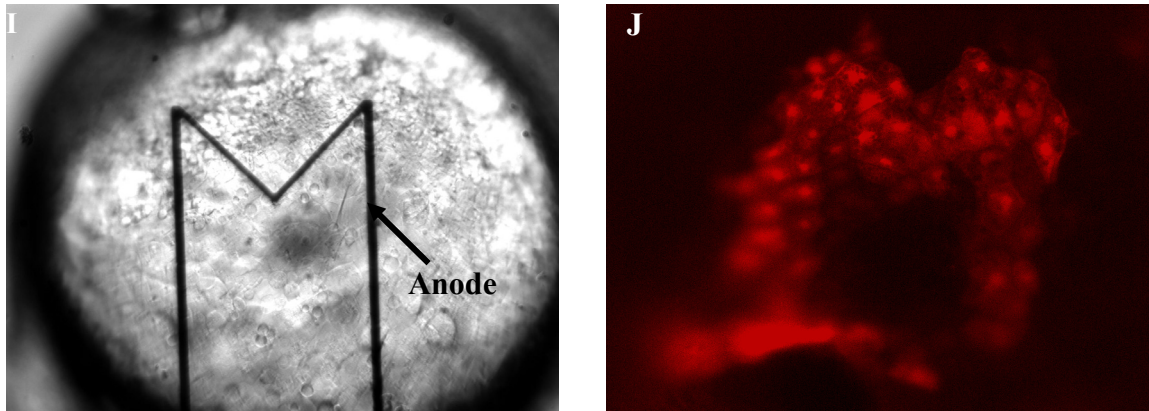
Figure 5.5: Fluorescent texas red was electroporated in various shapes in the yolk of zebrafish embryos at 10hpf. 10µm wide electrodes were designed in various shapes and used as anodes. a) A white light image of a line electrode with embryo on top. Most of the metal was covered with PDMS to shield electric field and hence acts as a point electrode. b) Fluorescent image of a point on the yolk. To increase the point dosing resolution, we designed the micropore devices. c) 10 µm wide line anode. d) A fluorescent image of a line electrode having been electroporated into the yolk (Once the embryos were pipetted into a clean dish for fluorescent imaging, they were not touched and hence are not oriented to the white light image). e) A white light image of an 'O' ring pattern. f) Fluorescent image of an 'O' ring. g) White light image of embryo sitting on two electrodes (anodes). h) Fluorescent image of embryo with two lines patterned on the embryo. i) White light image of 'M' shaped design. j) Fluorescent image of the 'M' pattern. Two square pulses of 10 V, 50 ms pulse width were used. Scale bar is 200 µm.

5.5.2 DNA and mRNA delivery

To demonstrate the successful delivery of biologically active molecules with this device, we first electroporated GFP-DNA and GFP-mRNA vectors into young zebrafish embryos and recorded the resultant expression of green fluorescent protein (GFP). In Figures 5.6a and 5.6b, 0.250 µg/µl solution of pCS2eGFP DNA was pipetted in the chamber and a 3 hpf embryo was placed on the electrode. Electroporation was performed and pCS2eGFP DNA entered the cells where it integrated with the nucleus and expressed itself. Fig. 5.6d shows the fluorescence from GFP at 24 hpf expressed by the DNA

sequestered inside dosed cells. No patterns could be formed on blastula stage cells as it takes 4-6 hrs for the DNA to integrate itself with the zebrafish and any pattern was lost during this time as cells divide continuously. Embryos treated in this way developed normally into fish.

We then used the above setup to electroporate patterned lines both at the yolk sac and at the brain region of older developing zebrafish. A single square pulse of 10 V, 100 ms pulse width was sufficient to deliver DNA into zebrafish at 24 hpf.
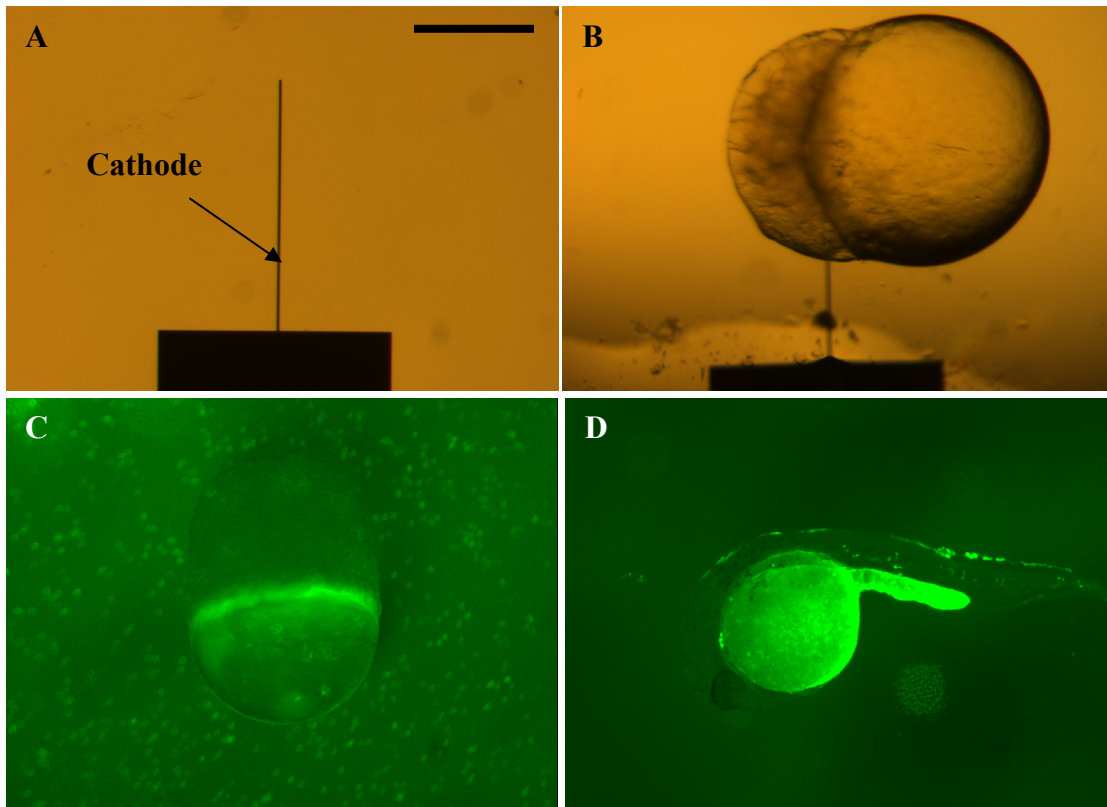
Figure 5.6: **Delivery of pCS2eGFP DNA in early stage developing embryos. a) 10 μm wide microfabricated platinum electrode acted as cathode during electroporation. b) 0.250 μg/μl of pCS2eGFP DNA was pipetted on top of the cathode and late blastula stage embryo (3 hpf) was placed in it. A probe tip was placed on top of the embryo to act as anode (not shown in the picture). Gap between two electrodes was 500 μm. One single square pulse of 10 V, 100 ms was delivered between the electrodes. c) 7 hpf developing embryo with dosed YSL. d) 24 hpf zebrafish after DNA integrated with the cell nucleus and spread in the entire fish as the fish developed. Scale bar is 200 μm.**

Figure 5.7 shows the same patterned electrode being used to deliver DNA-GFP in the shape of a line to a 24 hpf embryo. Figures 5.7a and 5.7b represent white light and fluorescent images of zebrafish at 48 hpf. A gap of 24 hrs ensured proper integration of DNA to the nucleus. The dotted red lines indicate the position of the cathode during dosing. In this case, the cathode was aligned parallel to the dorsal-ventral axis of the zebrafish. Figures 5.7c and 5.7d present a close-up top view of the same fish. Figures 5.7e and 5.7f present white light and fluorescent results for a second zebrafish. In this case, the cathode was aligned perpendicular to ventral-dorsal axis. Zebrafish dosed with DNA-GFP always exhibited the mosaic expression seen in Figures 5.7b, 5.7d, and 5.7f in which some but not all cells along the pattern expressed GFP. This was expected and correlates with whole-embryo electroporation (where not all cells are known to express the dosed genetic material). This is usually attributed to the fact that injected DNA, unlike injected mRNA, must enter not just the cell membrane, but also the cell nucleus and be transcribed efficiently. It is generally assumed that this mosaic pattern is due to the DNA being excluded from the nuclei of the non-expressing cells [139]. Increased expression percentage can be achieved by using a higher concentration of DNA but excessive DNA can lead to increased cell toxicity. Alternatively, there are known sequences (virus- or transposon-related factors) that can increase the merging percentage of the chromosomal DNA and dramatically increase the uniformity of the pattern (less mosaic) [139]. We also demonstrated how the devices could be used to deliver single points in a developing embryo (as with conventional electroporation or microinjection).
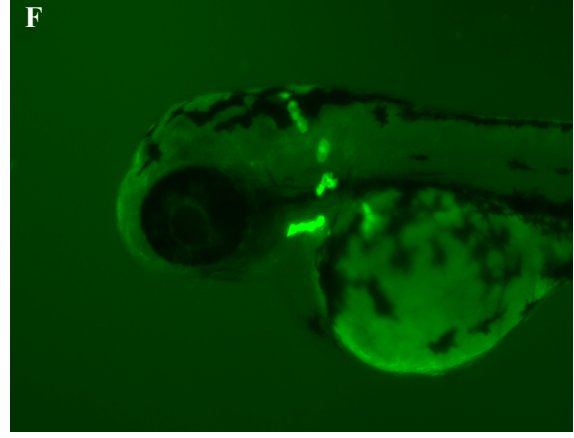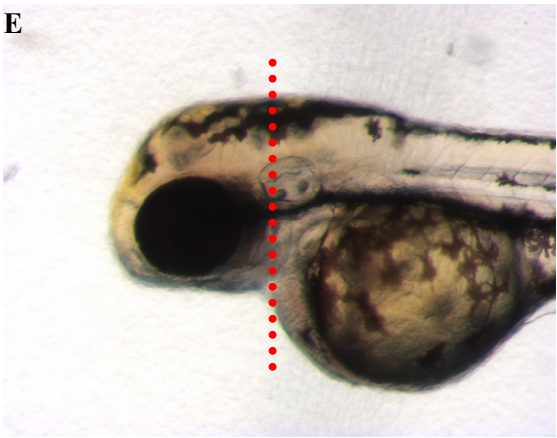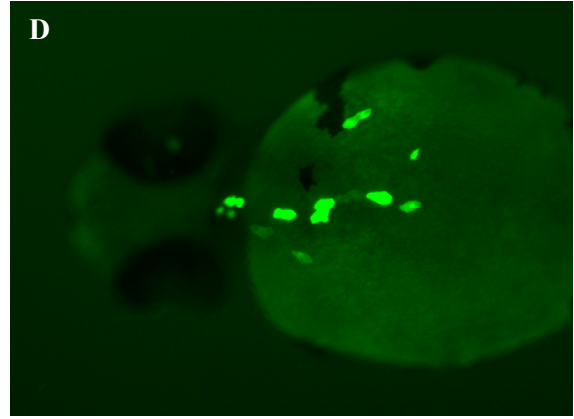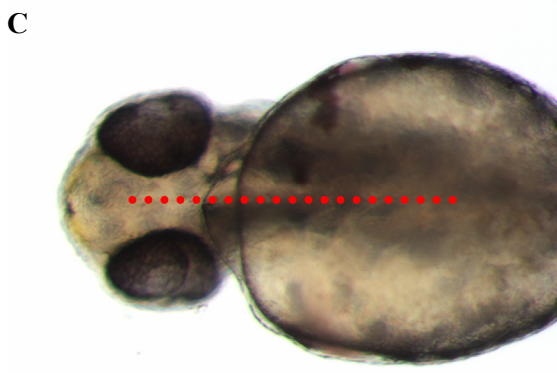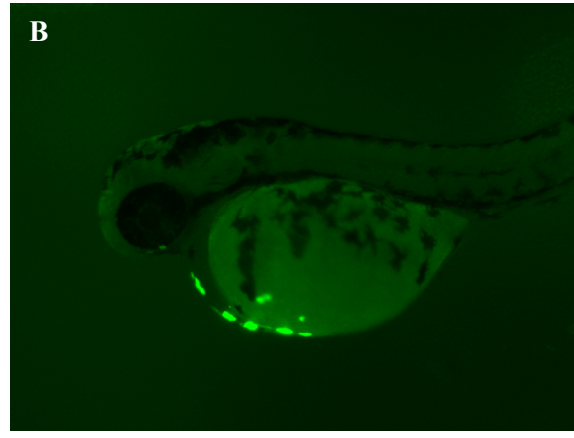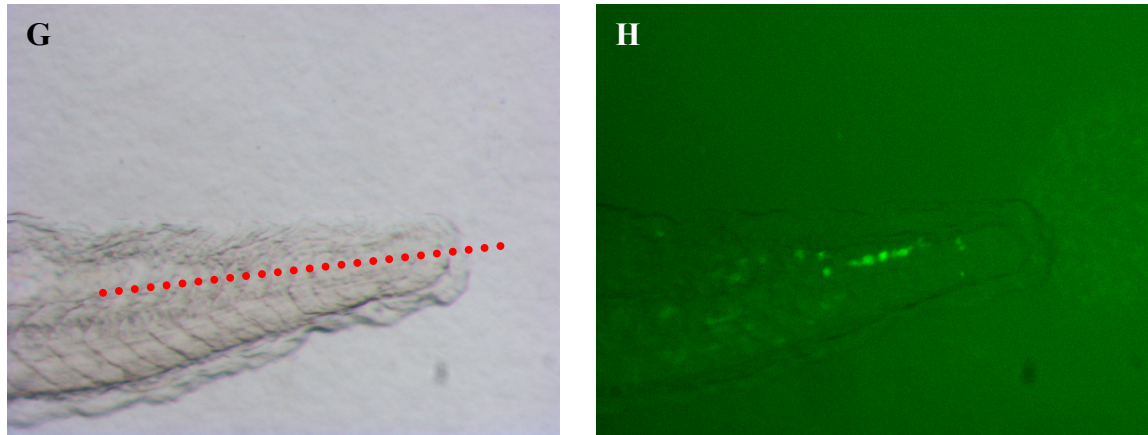
Figure 5.7: Delivery of pCS2eGFP in late stage zebrafish embryos in a line pattern. a) A 24 hpf zebrafish was positioned on top of the cathode. A cross-section view in white light of the pCS2eGFP DNA dosed embryo is shown. The red dotted line indicates where the electrode was placed. Electrode was placed parallel to the ventral-dorsal axis b) A fluorescent image of the dosed embryo. Typical 'mosaic' expression pattern was obtained. c) A top-view of the same fish in normal light. d) Fluorescent image taken from the top view e) White light image of a second zebrafish where the electrode was placed perpendicular to the ventral-dorsal axis f) Fluorescent image of zebrafish. g) White light image of the tail. Zebrafish somitogenesis is governed by a segmentation clock that generates oscillations in expression of several Notch pathway genes. Chevron-shaped areas within the tailbud where the clock is set up have been identified. h) Fluorescent image of the dosed zebrafish tailbud. Scale bar is 200 μm.

In Figure 5.8a, the majority of the cathode was passivated with PDMS, exposing only a small 10 μm x 10 μm area at the tip. The expression from the resultant dosed cell is shown in Figures 5.8c and 5.8d.

Introduction of in-vitro transcribed mRNA is a common technique to gain insight into the in-vivo activity of newly isolated cDNAs and has been the most commonly used method to express proteins in zebrafish embryos [139, 140]. Unlike dosed DNA, GFP expression from extracellular mRNA is non-mosaic, showing that most embryonic cells have received and translated the transcript. This relatively uniform expression and low

degree of mosaicism means that mRNA is well suited to studying effect on a large

number of cells and for studying events in early development which start as early as 3 hpf.
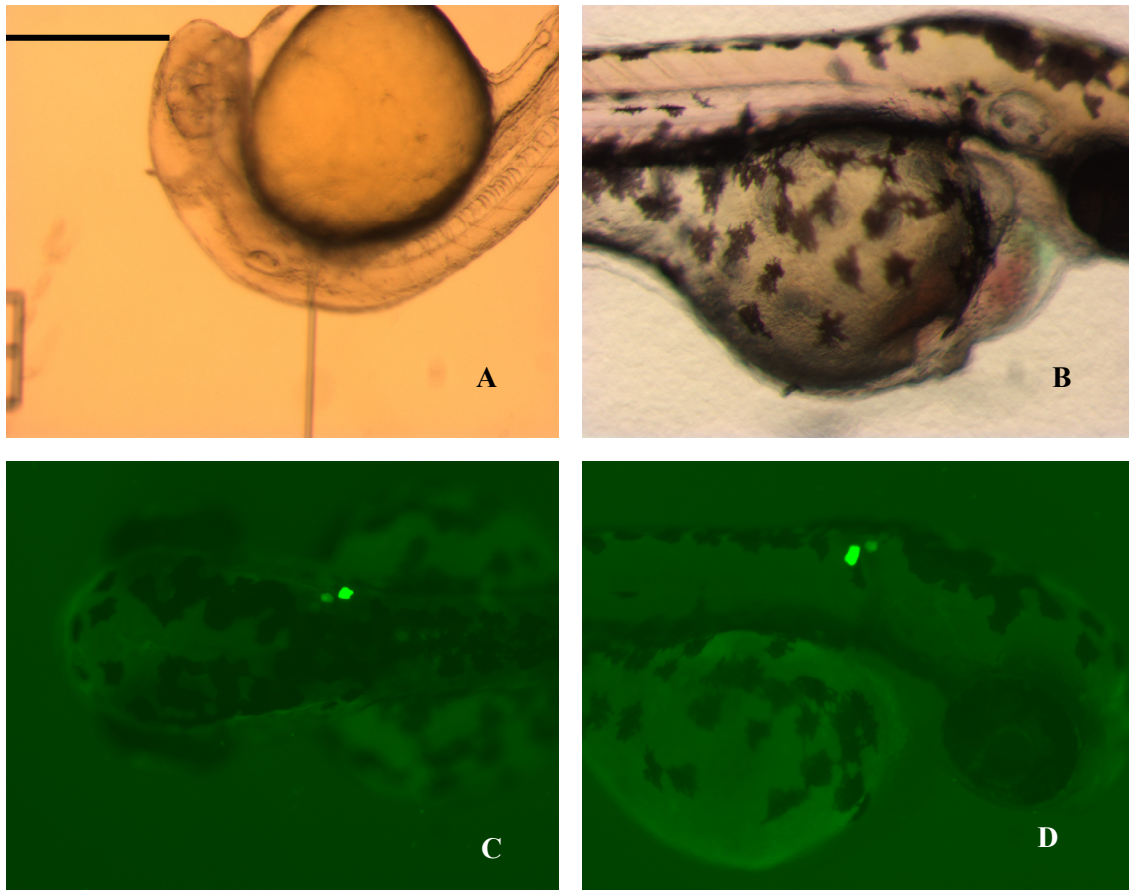
Figure 5.8:   **Point dosing of the pCS2eGFP DNA was achieved by shielding most of the electrode with PDMS. a) A 24 hpf zebrafish was positioned on top of cathode and electroporation conducted. b) A cross-section view of the zebrafish under white light at 30 hpf c) Fluorescent image of point dose delivered to the embryo (Top view) c) A fluorescent image of the point dose delivered to the embryo. Scale bar is 200 µm.**

To demonstrate successful delivery of mRNA, a 0.50 µg/µl solution of GFP-mRNA was

pipetted in the chamber and a single square pulse of 20 V and 50 ms pulse width was

applied. Figure 5.9a presents the white light image of where the electrode was placed and

Figure 5.9b presents the fluorescent image of the line pattern.
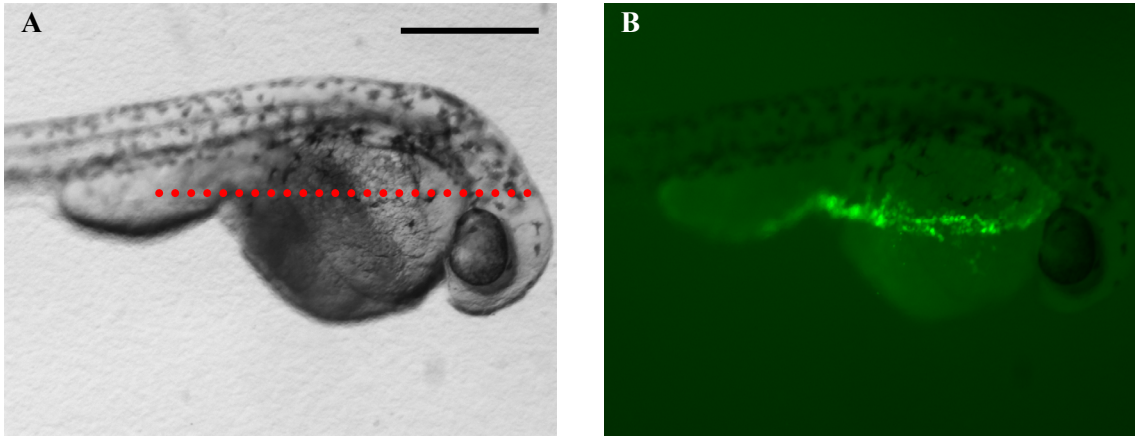
Figure 5.9: GFP-mRNA was electroporated in a line shape in a 24 hpf zebrafish. Red dotted line shows the location of electrode. Single pulse of 20 V, 50 ms pulse width was sufficient to deliver the mRNA. 0.50 µg/µl solution was used. a) White light image of the zebrafish. b) Fluorescent image of the zebrafish. Scale bar is 200 µm.

Lastly, we wish to explore microfluidic modifications which allowed the devices to dose more than one compound at a time. These microfluidic devices were constructed as long hollow gold channels on a glass substrate with a 10µm x 10 µm micropore etched in the roof of the channel. In this setup, the top gold channel, acted as an anode with a distant metal wire acting as cathode. Different solutions could be introduced into each channel via capillary action.

In Figure 5.10, a solution of 30 mM Texas Red and Fluoroscein Dextran mixed with E3 was introduced at the inlets and filled the channels as seen in Figures 5.10b and 5.10d. Embryos were positioned on top of the micropore array. A single pulse of 10 V, 100 ms pulse width was applied. Figures 5.10c and 5.10e show an embryo dosed via the micropore electrodes. Having a smaller molecular weight, fluorescein diffuses faster than texas red as seen in Fig. 5.10e. The resolution of point-dosing using this method is
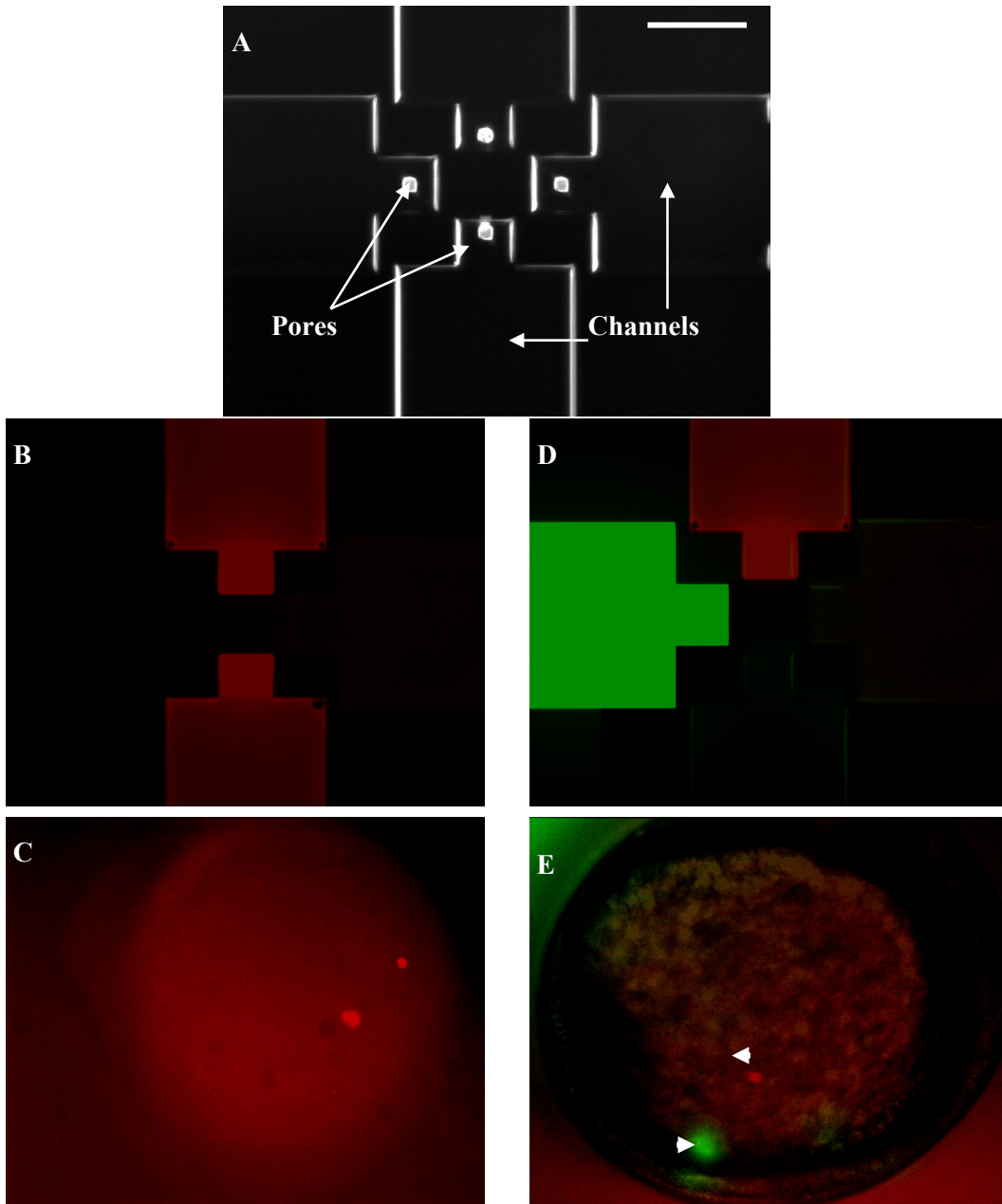
Figure 5.10: **A second microfluidic device of 10µm x 10µm micropore arrays was fabricated. a) Channels were fabricated. b) Texas red was introduced at the inlet and filled two channels via capillary action c) Fluorescent image of embryo after electroporation was conducted. Two separate dosing points were clearly visible d) Two separate dyes: fluorescein dextran and texas red were introduced at the inlet e) Two separate dosed points were visible as shown by arrowheads (ImageJ was used to superimpose two separate fluorescent dyes onto the same image). Scale bar is 200 µm.**

comparable to conventional microinjection techniques. These types of pores can themselves be made to open and close mechanically, controlling diffusion of the dye into the medium. An array of dozens of mechanically closable electroporation pores (similar to that in Figure 5.10) has been built.

5.5.3 Survival Analysis

By visually imaging each electroporated embryo, rate of survival and rate of successful delivery of foreign molecules was determined. For chorionated embryos, only the embryos that survived 3 hrs after electroporation were deemed viable and counted. For dechorionated embryos, an embryo was only considered as having survived if the embryo was viable and it exhibited straight ventral-dorsal axis symmetry. Curved embryos were not counted and were considered non-viable.

Delivery rate was calculated only from the survived embryos. Table 1 shows the survival and delivery rate of trypan blue in chorionated embryos and GFP-DNA and

Molecule	Stage (hpf)	Optimized voltage protocol	Survival rate (%)	Successful Delivery rate (%)	n
Trypan blue	3[*]	20 V, 100 ms, 2 pulses	80	60	30
DNA	24[#]	10 V, 100 ms, 1 pulse	91.3	38	23
mRNA	24[#]	20 V, 50 ms, 1 pulse	89	50	27

Table 5.1: **Survival rate of 24 hpf zebrafish electroporated with various molecules is presented. The high survival rate can be attributed to low voltages and long pulse widths used in the experiment.** [*] **Chorionated embryos** [#] **Dechorionated embryos**

GFP-mRNA into dechorionated 24 hpf embryos under the described conditions. We believe that shorter voltages and high pulse widths than those used conventionally helped in increasing survivability and dosing efficiency respectively. Table 1 also includes other parameters such as embryo stages at which electroporation was conducted, voltage, pulse width, number of pulses and the number of embryos tested. Direct physical contact of the embryos with metal lines had minimal adverse effects on the survival of the zebrafish. Electrolytic bubbles were observed in some cases and resulted in movement of the fish due to the fish reacting to the pulse.

5.6 Conclusion

Recent zebrafish studies have shown the existence of spatial heterogeneous developmental programs which are difficult to modulate with existing experimental tools [123, 141]. We have demonstrated a system employing microfabricated platinum electrodes and silicone polymer capable of dosing two-dimensional spatial patterns of compounds into zebrafish. We presented the design, fabrication and results of these interfaces and demonstrated how this system could be used to 'draw' patterns of tracer molecules, mRNA and DNA into the blastula and yolk of zebrafish embryos (*Danio rerio*) at different stages of development. We also demonstrated an extension to the basic technology that delivers more than one compound at different locations simultaneously. We believe this technology can be a powerful tool in dynamic developmental biology studies and could provide a route towards more sophisticated multi-compound chemical interfaces for studying developmental organisms.

CHAPTER VI

CONCLUSION

The technical contributions and achievements of this work are summarized in this chapter and future work is proposed.

6.1 Summary of Thesis contributions

This thesis has described microtechnologies for the spatial and temporal delivery of gene constructs into developing embryos and cells. Multiple techniques were designed, developed and tested. The micropore array devices utilized electrostatic actuation to deliver pixel resolution compounds into developing zebrafish embryos and require very low voltages. The electroporation technique utilized simple microfabricated electrodes on a glass surface to deliver GFP-DNA and GFP-RNA into developed zebrafish embryos and E.coli cell colonies. The meaningful contributions of this work are as follows:

6.2 Design, development and application of electrostatic actuators

Electrostatic actuation is a well known technique in 'dry' MEMS. Its use has been limited in wet MEMS because of electrochemistry problems such as electrolysis and electrode polarization. Quantitative analysis was performed to design actuators that required low voltages and high frequency signal to shield the electric double layer. Two

types of devices were fabricated. All-metal roof devices were designed to deliver pixel style extracellular compounds into developing embryos. Elastomer-metal devices were fabricated which require no external pneumatics, run at low power and are integrable into large scale devices. These devices provide the basis for a robust method to design microfluidic valves and peristaltic pumps for liquid transport.

6.3 Delivery of gene constructs into developing embryos

The work described in this thesis provides a compelling platform to use electroporation as a technique to controllably deliver gene constructs into developing embryos. The main contributions of this portion of the thesis are in demonstrating spatial and temporal delivery of biomolecules in exact patterns into embryos. The design, fabrication and results of microfabricated interfaces for the patterned delivery of foreign molecules via electroporation into developing embryos was presented. Device fabrication required a single mask process where various electrode shapes were patterned on a glass substrate. The demonstration of this application included optimizing the electroporation conditions which depend upon the amplitude, frequency, shape and number of pulses of the applied potential. This system was used to 'draw' two-dimensional patterns of tracer molecules, DNA and mRNA into the yolk and cells of zebrafish embryos (*Danio rerio*) at different stages of development. The successful delivery of two-dimensional patterns of trypan blue (normal dye), texas red (fluorescent dye), pCS2eGFP DNA and GFP-mRNA in both chorionated and dechorionated embryos was also demonstrated. Both DNA and mRNA were expressed in the desired patterns subsequent to delivery. This simple technique offers the unique advantage of introducing foreign compounds at local sites

74

and in specific patterns unlike any other microsystem technique and provides a new tool to aid advanced studies in cellular development and morphogenesis.

6.4 Delivery of gene constructs into *E.coli* colonies

Microbial consortia is the association of two or more cell colonies to pool their resources and achieve a common goal. Studying consortia can lead to insightful information on co-evolution and stability of species in their microenvironment. The technique developed in this thesis enables the dynamic control of spatial microenvironment which cannot be achieved with the current tools at this time.

6.5 Future research topics

6.5.1 Electrostatic actuators

The development of these electrostatic actuators in the nanoscale regime can be very meaningful, challenging and interesting. Because of their ease of fabrication and low power requirements, these actuators can be embedded with CMOS circuitry at the nanoscale to develop complete microfluidic devices which can valve, pump and mix fluids enabling various mobile point-of-care technologies.

6.5.2 Microfabricated electroporators

The use of microfabricated electroporators has many areas that can be studied in the future. Some of them are presented here:

- Indium Tin Oxide (ITO) can be constructed for better visual access from both the top and bottom of the substrate and not be limited by the type of

microscopes available. Or, Ag/AgCl electrodes can be used to minimize electrolysis during experimentation.

- Morphogens are diffusible substances that play a significant role in the developmental mechanism. Currently, morphogens are introduced into developing embryos by means of beads which are injected and studied. The use of microfabricated electroporators to deliver morphogens in specific shapes and at specific locations to study tissue development can result in an advanced understanding of these mechanisms.

- A complete entrapment chamber can be built and integrated with the current electrodes to entrap other model organisms such as Drosophila embryos, C.Elegans and planarians. Further 'hacking' of these organisms can be explored via introducing growth factors at different locations or specific local gene expression can be prevented by electroporating RNAi.

- Microfabricated electroporators can be used to design more robust microbial consortia experiments. Current techniques are limited to fixed spatial distances between two interacting species. More dynamic co-evolution studies can be performed by changing spatial distances with these electroporators and delivering auxotrophs into cell colonies.

6.6 Concluding remarks

This thesis presented microtechnologies for the delivery of spatial and temporal gene constructs into developing embryos and cells. The electrostatic actuator array devices require low voltages and can be used to build microfluidic valves, pumps or deliver extracellular compounds into developing embryos. Planar electrodes can be

76

microfabricated on glass substrates and used as gene electroporators to deliver biomolecules controllably into developing embryos and study their developmental mechanisms further. Topics that warrant further attention were mentioned in the previous section. It is the authors aim that the electroporators developed in this thesis be refined to a point that they can be used with multiple types of organisms in ordinary biological laboratories as tools for further developmental study.

APPENDICES

APPENDIX A

PULL-IN VOLTAGE WITH WATER AS DIELECTRIC

This appendix presents the derivation of the pull-in voltage with water (or any liquid dielectric) and oxide (or any other dielectric) as dielectric. To begin, we consider a capacitor plate system as shown in Figure A.1. The top plate is movable and is held by a spring having a spring constant k. The bottom plate is fixed, insulated by a layer of oxide with thickness t_{ox} and separated from the top plate by an initial gap distance g (dielectric thickness). ε_{ox} is the relative permittivity of the solid insulating layer, ε_L is the relative permittivity of the water between the plates, A is the area of overlap between the two capacitive plates, and ε_0 is the absolute permittivity. When the two plates are supplied by a bias V, the top plate has a displacement x, and the electrostatic force F_{elec} is expressed as:

$$F_{elec} = \frac{-\varepsilon_0 A V^2}{2\left(\dfrac{t_{ox}}{\varepsilon_{ox}} + \dfrac{g-x}{\varepsilon_{rL}}\right)} \tag{A.1}$$
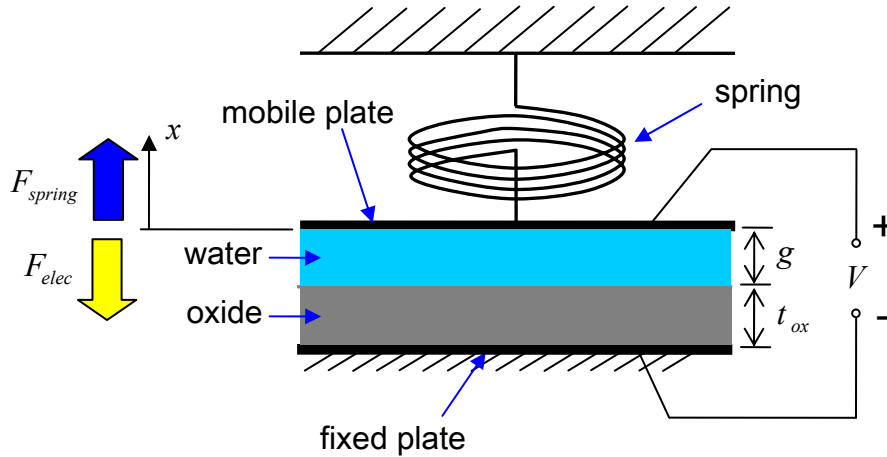
And the spring force F_{spring} on the top capacitor plate is expressed as:

79

$$F_{spring} = k \cdot x \tag{A.2}$$

Since the electrostatic force and spring force are equal and opposite, these forces are in equilibrium and can be written as:

$$F_{elec} + F_{spring} = 0 ;$$

$$\frac{-\varepsilon_0 A V^2}{2\left(\dfrac{t_{ox}}{\varepsilon_{ox}} + \dfrac{g-x}{\varepsilon_{rL}}\right)} + kx = 0 \tag{A.3}$$

Solve Equation (A.3) for voltage V :

$$V = \sqrt{\frac{2kx}{\varepsilon_{rL}\varepsilon_0 A}\left[(g-x) - \frac{t_{ox}\varepsilon_{rL}}{\varepsilon_{ox}}\right]} \tag{A.4}$$

To find the pull-in voltage, we need to find the location of extremum of (A.4) by differentiating it with respect to gap x :

$$\frac{\partial V}{\partial x} = 0 \tag{A.5}$$

Solving (A.5):

$$x = \frac{1}{3}\left(g + \frac{t_{ox}\varepsilon_{rL}}{\varepsilon_{ox}}\right) \tag{A.6}$$

Substituting (A.6) into (A.4), and the pull-in voltage V_{PI} can be then presented as:

$$V_{PI} = \sqrt{\frac{8k\left(g + t_{ox}\varepsilon_L/\varepsilon_{ox}\right)}{27\varepsilon_0\varepsilon_L A}} \tag{A.7}$$

FABRICATION PROCESS OF MICROPORE DEVICES

a

ITO electrodes   Dielectric

substrate

b

Via

substrate

c

Photoresist

substrate

d

Cr / Au seed layer

substrate

e

Electroplated Au

substrate

f

Etched pore   Exposed Area

substrate

g1

substrate

g2

substrate
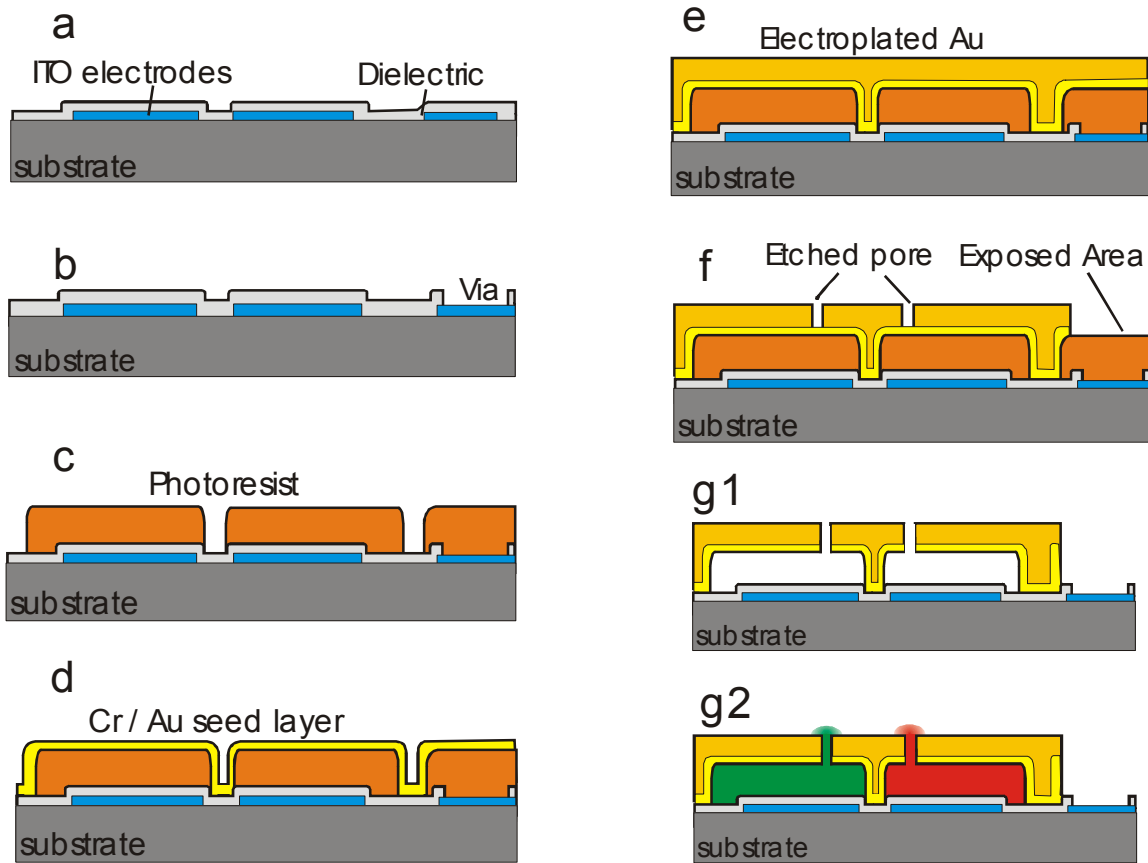
Process flow shows the fabrication of multi-compound dosing devices. a) Shipley®
1813 photoresist was spun at 1200 rpm, soft baked at 110 ºC for 1 minute and patterned.
Transparent indium tin oxide (ITO) was sputtered (1500 Å) and patterned through lift-off
process and annealed at 750 ºC in Rapid Thermal Anneal (RTA) oven. A thin layer of
oxide (0.45 µm) was via PECVD and annealed in RTA at 700 ºC. b) Contacts were time
wet etched through the oxide in 49% BHF (0.1 µm/min). c) A 5 µm Shipley® 1827
sacrificial photoresist was spun and patterned. d) A Cr/Au (150 Å /5000 Å) seed layer
was deposited. e) A 2 µm thick gold layer was electroplated to mechanically strengthen
the roof. f) Micropores were patterned lithographically and gold was wet etched. g1)

Sacrificial resist was removed by dipping the chip in acetone. g2) Channels were filled

with relevant compounds from different reservoirs prior to experimentation.

SCHEMATIC OF pCS2eGFP PLASMID

pCS2eGFP DNA was electroporated into developing zebrafish embryos. The preparation method is presented in Chapter IV. Here we present a schematic diagram of the plasmid.
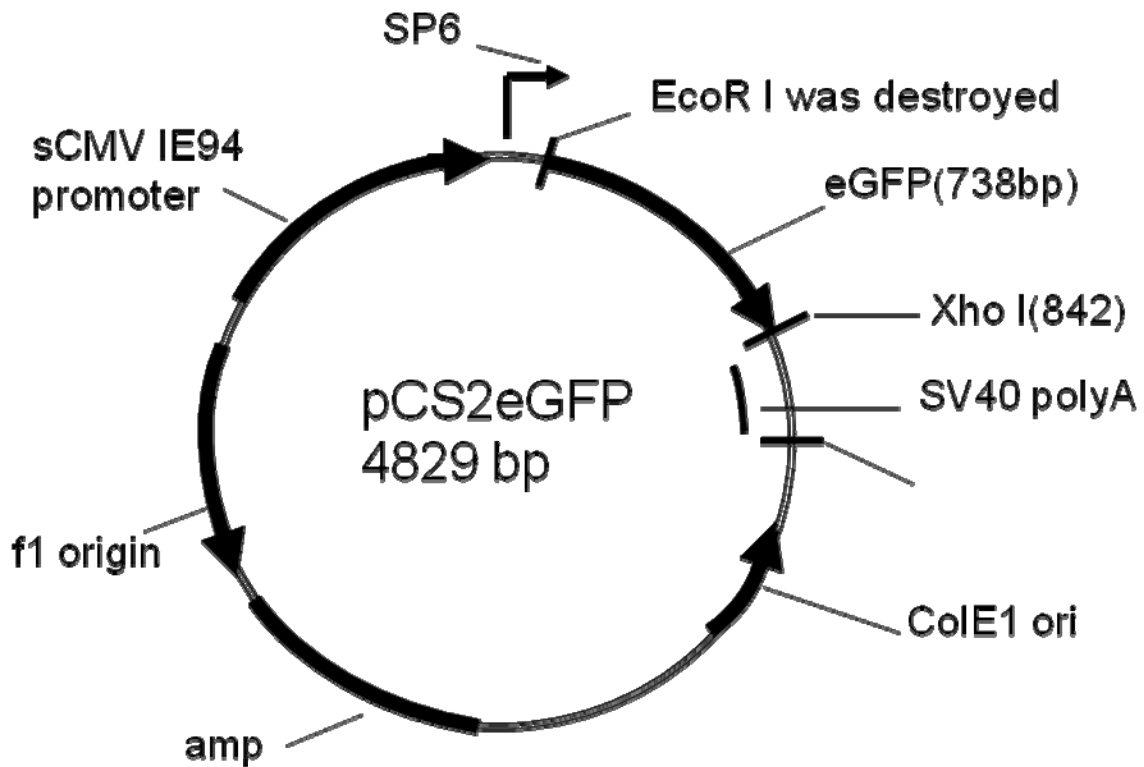
System water was obtained from the Duan lab and had the following characteristics: Temperature was kept at room temperature 28.5 ºC; pH was maintained at 7 – 8; conductivity was 700 – 800 μS.

BIBLIOGRAPHY

[1] L. Wolpert, "Positional information and the spatial pattern of cellular differentiation", *J. Theor. Biol.*, vol. 25, pp. 1 – 47, 1969.

[2] T. Gregor, D.W. Tank, E.F. Wieschaus and W. Bialek, "Probing the limits to positional information", *Cell*, vol. 130, pp. 153 – 164, 2007.

[3] C. Neumann and S. Cohen, "Morphogens and pattern formation", *Bioessays*, vol. 19, pp. 721 – 729, 1997.

[4] S.D. Podos and E.L. Ferguson, "Morphogen gradients: new insights from DPP", *Trends in Genetics*, vol. 15, pp. 396 – 402, 1999.

[5] L. Kodjabachian, "Morphogen gradients: Nodal enters the stage", *Current Biology*, vol. 11, pp. 655 – 658, 2001.

[6] W. Driever and C. Nüsslein-Volhard, "A gradient of Bicoid protein in *Drosophila* embryos", *Cell*, vol. 54, pp. 83 – 93, 1988.

[7] M. Zecca, K. Basler and G. Struhl, "Sequential organizing activities of engrailed, hedgehog and decapentaplegic in the Drosophila wing", *Development*, vol. 121, pp. 2265 – 2278, 1995.

[8] T. Ariizumi and M. Asashima, "Control of the embryonic body plan by activin during amphibian development", *Zoolog. Sci.*, vol. 12, pp. 509 – 521, 1995.

[9] G. Struhl, K. Struhl and P.M. Macdonald, "The gradient morphogen Bicoid is a concentration-dependent transcriptional activator", *Cell,* vol. 57, pp. 1259 – 1273, 1989.

[10] A. Ephrussi and D. St Johnston, "Seeing Is Believing: The Bicoid Morphogen Gradient Matures", *Cell*, vol. 116, pp. 143 – 152, 2004.

[11] K.M. Reilly and D.A. Melton, "Short-range signaling by candidate morphogens of the TGF beta family and evidence for a relay mechanism of induction", *Cell*, vol. 86, pp. 743 – 754, 1996.

[12] M.J. Mahoney and W.M. Saltzman, "Transplantation of brain cells assembled around a programmable synthetic microenvironment", *Nature Biotechnology*, vol. 19, pp. 934 - 939, 2001.

[13] T. Yasuda, T. Higashi and Y. Nakashima, "Fabrication of microfluidic device for axonal growth", *Transducers*, Boston, pp. 1259 - 1262, 2003.

[14] M.C. Peterman, J. Noolandi, M.S. Blumenkranz and H.A. Fishman, "Localized chemical release from an artificial synapse chip", *PNAS*, vol. 101, pp. 9951 – 9954, 2004.

[15] K. Brenner, L. You and F.H. Arnold, "Engineering microbial consortia: a new frontier in synthetic biology", *Trends in Biotechnology*, vol. 26, no. 9, pp. 483 – 489, 2008.

[16] S. Takayama, E. Ostuni, P. LeDuc, K. Naruse, D.E. Ingber and G.M. Whitesides, "Subcellular positioning of small molecules", *Nature*, vol. 411, 2001.

[17] S.K. Dertinger, D.T. Chiu, N.L. Jeon and G.M. Whitesides, "Generation of gradients having complex shapes using microfluidic networks", *Analytical Chemistry*, vol. 73, pp. 1240 – 1246, 2001.

[18] T.F. Kosar, A. Tourovskaia, X.Figueroa-Masot, M.E. Adams and A. Folch, "A nanofabricated planar aperture as a mimic of the nerve-muslce contact during synaptogenesis", *Lab chip*, vol. 6, pp. 632 – 638, 2006.

[19] M.A. Unger, H.P. Chou, T. Thorsen, A. Scherer and S.R. Quake, "Monolithic microfabricated valves and pumps by multilayer soft lithography", *Science*, vol. 288, pp. 113 – 116, 2000.

[20] E.M. Lucchetta, J.H. Lee, L.A. Fu, N.H. Patel and R.F. Ismagilov, "Dynamics of Drosophila embryonic patterning network perturbed in space and time using microfluidics", *Nature*, vol. 434, pp. 1134 – 1138, 2005.

[21] R.F. Ismagilov and M.M. Maharbiz, "Can we build synthetic, multicellular systems by controlling developmental signaling in space and time?", *Current Opinion in Chemical Biology*, vol. 11, pp. 604 – 611, 2007.

[22] O. Voiculescu, F. Bertocchini, L. Wolpert, R.E. Keller and C.D. Stern, "The amniote primitive streak is defined by epithelial cell intercalation before gastrulation", *Nature*, vol. 449, pp. 1049 – 1052, 2007.

[23] O. Voiculescu, C. Papanayotou and C.D. Stern, "Spatially and temporally controlled electroporation of early chick embryos", *Nature Protocol*, vol. 3, pp. 419 – 426, 2008.

[24] I.A. Shestopalov and J.K. Chen, "Chemical technologies for probing embryonic development", *Chem. Soc. Rev.*, vol. 37, pp. 1294 – 1307, 2008.

[25] Y. Kawakami, A. Raya, R.M. Raya, C. Rodriguez-Esteban, J. C. I. Belmonte, "Retinoic acid signalling links left–right asymmetric patterning and bilaterally symmetric somitogenesis in the zebrafish embryo", *Nature*, vol. 435, pp. 165 – 171, 2005.

[26] F.J. Vonk and M.K. Richardson, "Developmental biology: Serpent clocks tick faster", *Nature*, vol. 454, pp. 282 – 283, 2008.

[27] A. Mara, J. Schroeder, C. Chalouni and S.A. Holley, "Priming, initiation and synchronization of the segmentation clock by deltaD and deltaC", *Nat. Cell Biol.*, vol. 9, pp. 523 – 530, 2007.

[28] J.S. Eisen, "Zebrafish makes a big splash", *Cell*, vol. 87, pp. 969 - 977, 1996.

[29] T.H. Morgan, "An attempt to analyze the constitution of the chromosomes on the basis of sex-limited inheritance in Drosophila", *J .Exp. Zool.*, vol. 11, pp. 365 - 412, 1911.

[30] A.H. Sturtevant, "The linear arrangement of six sex-linked factors in *Drosophila*, as shown by their mode of association", *J. Exp. Zool.*, vol. 14, pp. 43 - 59, 1913.

[31] H.J. Muller, "The regionally differential effect of X rays on crossing over in autosomes of Drosophila", *Genetics*, vol. 10, pp. 470 - 507, 1925.

[32] A.C. Spradling and G.M. Rubin, "Genetic transformation of Drosophila with transposable element vectors", *Science*, vol. 218, pp. 348 - 353, 1982.

[33] D.C. Cannatella and R.O. Desa, "Xenopus-Laevis as a model organism", *Systematic Biology*, vol. 42, pp. 476 - 507, 1993.

[34] J. Domingo, J. Serratosa, C. Vidal and E. Rius, "Mitotic coincidence of chick embryo hepatocytes in vivo and the transition probability model of the cell cycle", *Nature*, 1978, vol. 273, pp. 50 - 52, 1978.

[35] D.J. Watts and S.H. Strogatz, "Collective dynamics of 'small-world' networks", *Nature*, vol. 393, pp. 440 - 442, 1998.

[36] S. Kamel-Reid *et al.*, "A model of human acute lymphoblastic leukemia in immune-deficient SCID mice", *Science*, vol. 246, pp. 1597 - 1600, 1989.

[37] K. Dooley and L.I. Zon, "Zebrafish: a model system for the study of human disease", *Current opinion in Genetics and Development*, vol. 10, pp. 252 – 256, 2000.

[38] N. Bahary and L.I. Zon, "Use of zebrafish (Danio rerio) to define hematopoiesis", *Stem cells*, vol. 16, pp. 89 – 98, 1998.

[39] C.B. Kimmel, W.W. Ballard, S.R. Kimmel, B. Ullmann and T.F. Schilling, "Stages of embryonic development of the zebrafish", *Dev. Dynamics*, vol. 203, pp. 253 – 310, 1995.

[40] C.B. Kimmel and R.D. Law, "Cell lineage of zebrafish blastomeres. II. Formation of the yolk syncytial layer", *Dev. Biol.*, vol. 108, pp. 86 - 93, 1985a.

[41] C.B. Kimmel and R.D. Law, "Cell lineage of zebrafish blastomeres. III Clonal analysis of the blastula and gastrula stages", *Dev. Biol.*, vol. 107, pp. 94 - 101, 1985b.

[42] E. Hanneman and M. Westerfield, "Pathfinding and synapse formation in a zebrafish mutant lacking functional acetylcholine receptors", *J. Comp. Neurol.*, vol. 284, pp. 350 - 361, 1989.

[43] S.J. Singer and G.L. Nicolson, "The fluid mosaic model of the structure of cell membranes", *Science*, vol. 175, pp. 720 - 731, 1972.

[44] S.J. Singer, "The structure and function of membranes – a personal memoir", *Journal of Membrane Biology*, vol. 129, pp. 3 - 12, 1992.

[45] M. Hagedorn, F.W. Kleinhans, D. Artemov and U. Pilatus, "Characterization of a major permeability barrier in the Zebrafish embryo", *Biology of reproduction*, vol. 59, pp. 1240 - 1250, 1998.

[46] D.M. Rawson, T. Zhang, D. Kalicharan and W.L. Jongebloed, "Field emission scanning electron microscopy studies of the chorion, plasma membrane and syncytial layers of the gastrula-stage embryo of the zebrafish Brachydanio rerio: a consideration of the structural and functional relationship with respect to cryoprotectant penetration", *Aquaculture Research*, vol. 31, pp. 325 - 336, 2000.

[47] T. Zhang and D.M. Rawson, "Feasibility studies on vitrification of intact zebrafish (Brachydanio rerio) embryos", *Cryobiology*, vol. 33, pp. 1 - 13, 1996.

[48] M. Hagedorn *et al.*, "Magnetic resonance microscopy and spectroscopy reveal kinetics of cryoprotectant permeation in a multicompartmental biological system", *PNAS*, vol. 93, pp. 7454 - 7459, 1996.

[49] M. Hagedorn *et al.*, "Chill sensitivity and cryoprotectant permeability of dechorionated zebrafish embryos, *Brachydanio rerio", Cryobiology*, vol. 34, pp. 251 - 263, 1997.

[50] S. Rieger, R.P. Kulkarni, D. Darcy, S.E. Fraser and R.W. Koster, "Quantum dots are powerful multipurpose vital labeling agents in zebrafish embryos", Dev. Dyn., vol. 234, pp. 670 – 681, 2005.

[51] J.G. Cloud, "Strategies for introducing foreign DNA into the germ line of fish", J. Reprod. Fertil. Suppl., vol. 41, pp. 107 – 116, 1990.

[52] P. Culp, C. Volhard and N. Hopkins, "High frequency germ line transmission of plasmid DNA sequences injected into fertilized zebrafish eggs", *PNAS*, vol. 88, pp. 7953 – 7958, 1991.

[53] D.A Powers, L. Hereford, T. Cole, T.T. Chen, C.M. Lin, K. Kight, K. Creech and R. Dunham, "Electroporation: A method for transferring genes into the gametes of zebrafish

(Brachydanio rerio), channel catfish (Ictalurus punctatus) and common carp (Cyprinus carpio)", *Mar. Mol. Biol. Biotechnology*, vol. 1, pp. 301 – 308, 1992.

[54] M. Janik, F.W. Kleinhans and M. Hagedorn, "Overcoming a permeability barrier by microinjecting cryoprotectants into zebrafish embryos (Brachydanio rerio)", *Cryobiology*, vol. 41, pp. 25 – 34, 2000.

[55] U.K. Tirlapur and K. Konig, "Targeted transfection by femtosecond laser", *Nature*, vol. 418, pp. 290 – 292, 2002.

[56] U.K. Tirlapur and K. Konig, "Femtosecond near-infrared laser pulses as a versatile non-invasive tool for intra-tissue nanoproecessing in plants without compromising viability", *Plants J.*, vol. 31, pp. 365 – 374, 2002.

[57] G.W. Stuart, J.V. McMurray and M. Westerfield, "Replication, integration and stable germ-line transmission of foreign sequences injected into early zebrafish embryos", *Development*, vol. 103, pp. 403 – 412, 1988.

[58] A. Amsterdam, S. Lin and N. Hopkins, "The *Aequorea Victoria* green fluorescent protein can be used as a reported in live zebrafish embryos", *Dev. Biol.*, vol. 171, pp. 123 – 129, 1995.

[59] Q. Xu, "Microinjection into Zebrafish embryos", *Molecular Methods in Developmental biology: Xenopus and Zebrafish*, vol. 127, pp. 125 – 132, 1999.

[60] C.B. Kimmel, R.M. Warga and T.F. Schilling, "Origin and organization of the zebrafish fate map", *Development*, vol. 108, pp. 581 - 594, 1990.

[61] R.K. Ho, "Cell movements and cell fate during zebrafish gastrulation", *Development,* pp. 65 - 73, 1992.

[62] G.W. Stuart, J.V. McMurray and M. Westerfield, "Replication, integration and stable germ-line transmission of foreign sequences injected into early zebrafish embryos", *Development*, vol. 103, pp. 403 – 412, 1988.

[63] G.W. Stuart, J.R. Vielkind, J.V. McMurray and M. Westerfield, "Stable lines of transgenic zebrafish exhibit reproducible patterns of transgene expression", *Development*, vol. 109, pp. 557 – 584, 1990.

[64] W. Wang, X. Liu, D. Gelinas, B. Ciruna and Y. Sun, "A fully automated robotic system for microinjection of zebrafish embryos", *PLoS ONE*, vol. 2, 2007.

[65] L. Lin and A.P. Pisano, "Silicon processed microneedles", *J. Microelectromech. System*, vol. 8, pp. 78 – 84, 1999.

[66] K. Chun, G. Hashiguchi, H. Toshiyoshi and H. Fujita, "Fabrication of array of hollow microcapillaries used for injection of genetic materials into animal/plant cells", *Japan. J. Appl. Phys.*, vol. 38, pp. 279 – 281, 1999.

[67] S. Zappe, M. Fish, M.P. Scott and O. Solgaard, "Automated MEMS based Drosophila embryo injection system for high-throughput RNAi screens", *Lab Chip*, vol. 6, pp. 1012 – 1019, 2006.

[68] M.A. Ben´ıtez, J.A. Plaza, S.Q. Sheng and J. Esteve, " A new process for releasing micromechanical structures in surface micromachining", *J. Micromech. Microeng.*, vol. 6, pp. 36–38, 1996.

[69] Z. Xiao *et al.*, "A new release process for polysilicon surface micromachining using sacrificial polysilicon anchor and photolithography after sacrificial etching", *J Micromech. Microeng.*, vol. 9, pp. 300 – 304, 1999.

[70] D.V. McAllister, P.M. Wang, S.P. Davis, J.H. Park, P.J. Canatella, M.G. Allen and M.R. Prausnitz, "Microfabricated needles for transdermal delivery of macromolecules and nanoparticles: Fabrication methods and transport studies", PNAS, vol. 100, pp. 13755 – 13760, 2003.

[71] K. Oka, A. Seiji, Y. Arai and Y. Isono, "Fabrication of a Microneedle for a Trace Blood Test", *Sens. Actuators A*, vol. 97–98, pp. 478 – 485, 2002.

[72] K. Chun, G. Hashiguchi, H. Toshiyoshi and H. Fujita, "Fabrication of array of hollow microcapillaries used for injection of genetic materials into animal/plant cells", *Japan. J. Appl. Phys.*, vol. 38, pp. 279 – 281, 1999.

[73] J. Chen and K. D. Wise, "A multichannel neural probe for selective chemical delivery at the cellular level", *IEEE Trans. Biomed. Eng.*, vol. 44, pp. 760 – 769, 1997.

[74] E.J. Droog, J. Henricson, G.E. Nilsson and F. Sjoberg, "A protocol for iontophoresis of acetylcholine and sodium nitroprusside that minimizes nonspecific vasodilatory effects", *Microvascular Research*, vol. 67, pp. 197 – 202, 2004.

[75] P.G. Green, "Iontophoretic delivery of peptide drugs", *J.Control Release*, vol. 41, pp. 33 – 48, 1996.

[76] J. Singh and K.S. Bhatia, "Topical iontophoretic drug delivery: pathways, principles, factors, and skin irritation", *Med. Res. Rev.*, vol. 16, pp. 285 – 296, 1996.

[77] P. Singh and H.I. Maibach, "Iontophoresis in drug delivery: basic principles and applications", *Crit. Rev. Ther. Drug Carr. Syst.*, vol. 11, pp. 161 – 213, 1994.

[78] R.I. Dorsky, R.T. Moon and D.W. Raible, "Environmental signals and cell fate specification in premigratory neural crest", *BioEssays*, vol. 22, pp. 708 – 716, 2000.

[79] M.N. Berlinger, "Skin microcirculation during tapwater iontophoresis in humans: cathode stimulates more than anode", *Microvasular Research*, vol. **54**, pp. 74 – 80, 1995.

[80] M. Grossman *et al.*, "The effect of iontophoresis on the cutaneous microvasculature: evidence for current-induced hyperemia", *Microvascular Research*, vol. **50**, pp. 444 – 452, 1995.

[81] M.M. Hanneman, W.G. Lidell, A.C. Shore, M. Clark and J.E. Tooke, "Vascular function in women with previous gestational diabetes mellitus", *J. Vascular Research*, vol. **39**, pp. 311 – 319, 2002.

[82] S.J. Morris and A.C. Shore, "Skin blood flow responses to the iontophoresis of acetylcholine and sodium nitroprusside in man: possible mechanisms", *J. Physiol.*, vol. **496**, pp. 531 – 542, 1996.

[83] S.J. Morris, A.C. Shore and J.E. Tooke, "Responses of the skin microcirculation to acetylcholine and sodium nitroprusside in patients with NIDDM", *Diabetologia*, vol. **38**, pp. 1337–1344, 1995.

[84] K.M. Rambabu, S.H. Narayana Rao and N.M. Rao, *BMC Biotechnology*, vol. 5, pp. 362 – 368, 2005.

[85] P.F. Lurquin, "Gene transfer by electroporation", *Molecular Biotechnology*, vol. 7, pp. 5 – 35, 1997.

[86] E. Neumann, M. Schaefer-Riddler, Y. Wang and P.H. Hofschneider, "Gene transfer into mouse lyoma cells by electroporation in high fields", J. EMBO, vol. 1, pp. 841 – 845, 1982.

[87] R.D. Jamieson, M.P. Boder, P.B. Boder and D.Baran, "Simulation and experimental demonstration of the electric field assisted microchip for *in vitro* gene delivery enhancement", *IEEE Proc.*, vol. 136, pp. 41 – 44, 1989.

[88] R.A. Meldrum, M. Bowl, S.B. Ong and S. Richardson, "Optimisation of electroporation for biochemical experiments in live cells", *Biochem. Biophys. Res. Commun.*, vol. 256, pp. 235 – 239, 1999.

[89] H. Lambert, R. Pankov, J. Gauthier and R. Hancock, "Electroporation mediated uptake of proteins into mammalian cells", *Biochem.Cell Biol.*, vol. 68, pp. 729 – 734, 1990.

[90] A.K. Banga and M.R. Prausnitz, "Assessing the potential of skin electroporation for the delivery of protein and gene based drugs", Trends in biotechnology, vol. 16, pp. 408 – 412, 1998.

[91] G.A. Cerda, J.E. Thomas, M.L. Allende, R.O. Karlstrom and V. Palma, "Electroporation of DNA, RNA and morpholinos into zebrafish embryos", *Methods*, vol. 39, pp. 207 – 211, 2006.

[92] O. Voiculescu, C. Papanayotou and C. Stern, "Spatially and temporally controlled electroporation of early chick embryos", *Nature Protocols*, vol. 3, pp. 419 – 426, 2008.

[93] O. Voiculescu, F. Bertocchini, L. Wolpert, R.E. Keller and C.D. Stern, "The amniote primitive streak is defined by epithelial cell intercalation before gastrulation", *Nature*, vol. 449, pp. 1049 – 1052, 2007.

[94] K. Konig, I. Riemann, W. Fritzsche, "Nanodissection of human chromosomes with near-infrared femtosecond laser pulses", *Optical Letters*, vol. 26, pp. 819 – 821, 2001.

[95] V. Kohli, V. Robles, M.L. Cancela, J.P. Acker, A.J. Waskiewicz and A.Y. Elezzabi, "An alternative method for delivering exogenous material into developing zebrafish embryos", *Biotechnology and Bioengineering*, vol. 98, pp. 1230 – 1241, 2007.

[96] S.G. Chaulk and A.M. MacMillan, "Caged RNA: photo control of a ribozyme reaction", *Nucleic Acids Res.*, vol. 26, pp. 3173 – 3178, 1998.

[97] H. Ando, T. Furuta, R.Y. Tsien and H. Okamoto, "Photo-mediated gene activation using caged RNA/DNA in zebrafish embryos", *Nature genetics*, vol. 28, pp. 317 – 325, 2001.

[98] P.Y. Chiou, A.T. Ohta and M.C. Wu, "Massively parallel manipulation of single cells and microparticles using optical cells", *Nature*, vol. 436, pp. 370 – 372, 2005.

[99] J.K. Valley, A. Jamshidi, A.T. Ohta, H-Y Hsu and M.C. Wu, "Operational regimes and physics present in optoelectronic tweezers", *JMM*, vol. 17, pp. 342 – 350, 2008.

[100] M. Janik, F.W. Kleinhans and M.M. Hagedorn, "Overcoming a permeability barrier by microinjecting cryoprotectants into zebrafish embryos (Brachydanio rerio)", *Cryobiology*, vol. 41, pp. 25 – 34, 2000.

[101] S.C. Terry, J.H. Jerman and J.B. Angell, "A gas chromatographic air analyzer fabricated on silicon wafer", *IEEE Trans. Electron Devices*, vol. 26, pp. 1880 – 1886, 1979.

[102] K. Sato and M. Shikida, "An electrostatically actuated gas valve with an S-shaped film element", *J. Micromech.Microeng.,*vol. 4, pp. 205 – 209, 1994.

[103] H. Jerman, "Electrically-activated normally closed diaphragm valves", *J. Micromech. Microeng.*, vol. 4, pp. 210 – 216, 1994.

[104] H.Q. Li, D.C. Roberts, J.L. Steyn, K.T. Turner, O. Yaglioglu, N.W. Hagood, S.M. Spearing, M. Schmidt, "Fabrication of a high frequency piezoelectric microvalve", *Sensors and Actuators A*, vol. 111, pp. 51 – 56, 2004.

[105] M. Shikida, K. Sato, S. Tanaka, Y. Kawamura and Y. Fujisaki, "Electrostatically driven gas valve with high conductance", *J. Microelectromech. Syst.*, vol. 3, pp. 76 – 80, 1994.

[106] C. Goll *et al.*, "An electrostatically actuated polymer microvalve equipped with a movable membrane electrode", *J. Micromech. Microeng.*, vol. 7, pp. 224 – 226, 1997.

[107] M.A. Unger, H.P. Chou, T. Thorsen, A. Scherer and S.R. Quake, "Monolithic microfabricated valves and pumps by multilayer soft lithography", *Science*, vol. 288, pp. 113 – 116, 2000.

[108] R.A. Mathies *et al.*, Proc. 2002 Solid-State Sensor, Actuator, and Microsystems Workshop (Hilton Head Island, SC), June 2 – 6, pp. 112–117, 2002.

[109] W.H. Grover, A.M. Skelley, C.N. Liu, E.T. Lagally and R.A. Mathies, "Monolithic membrane valves and diaphragm pumps for practical large scale integrated into glass microfluidic devices", *Sensors and Actuators B: Chemical*, vol. 89, pp. 315 – 323, 2003.

[110] S-K. Fan, P-P de Guzman and C.J. Kim, Proc. 2002 Solid-State Sensor, Actuator, and Microsystems Workshop (Hilton Head Island, SC), June 2 – 6, pp. 134 – 137, 2002.

[111] W.H. Grover, R.H.C. Ivester, E.C. Jensen and R. A. Mathies, "Development and multiplexed control of latching pneumatic valves using microfluidic logical structures", *Lab Chip*, vol. 5, pp. 623 – 631, 2006.

[112] T. Thorsen, S.J. Maerkl and S.R. Quake, "Microfluidic Large-Scale Integration", *Science*, vol. 298, pp. 580 – 582, 2002.

[113] N.A. Cellar and R.T. Kennedy, "A capillary-PDMS hybrid chip for separations-based sensing of neurotransmitters in vivo", *Lab Chip*, vol. 6, pp. 1205 – 1212, 2006.

[114] J. Xie, J. Shih, Q. Lin, B. Yang and Y-C. Tai, "Surface micromachined electrostatically actuated micro peristaltic pump", *Lab Chip*, vol. 4, pp. 495 – 501, 2004.

[115] A-S. Rollier, B. Legrand, D. Collard and L. Buchaillot, "The stability and pull-in voltage of electrostatically parallel-plate actuators in liquid solutions", *J. Micromech. Microeng.*, vol. 16, pp. 794 – 801, 2006.

[116] K.R. Zavadil, M.A. Rising and P.C. Galambos, Proc. Electrochemical Society Microfabricated Systems and MEMS VI, SeriesPV2002–6, Pennington, NJ, pp. 44 – 152, 2002.

[117] J.W. Judy, "Microelectromechanical systems (MEMS) fabrication, design and applications", *Smart Material Structure*, vol. 10, pp. 1115 – 1134, 2001.

[118] T.L. Sounart, T.A. Michalske and K.R. Zavadil, "Frequency dependent electrostatic actuation in microfluidic MEMS", *J. Microelectromechanical Systems*, vol. 14, pp. 125–133, 2005.

[119] B. Legrand, A.-S. Rollier, D. Collard and L. Buchaillot, "Suppression of the pull-in instability for parallel-plate electrostatic actuators operated in dielectric liquids", *Applied Physics Letter*, vol. 88, 2006.

[120] W.C. Young, Roark's Formulas for Stress and Strain, McGraw-Hill International Edition, 1989.

[121] Dow Corning® WL-5150 and WL-5351 product information.

[122] C-W. Baek, Y-K. Kim, Y. Ahn and Y-H. Kim, "Measurement of the mechanical properties of electroplated gold thin films using micromachined beam structures," *Sensors and Actuators A*, vol. 117, pp. 17 – 27, 2005.

[123] R.F. Ismagilov and M.M. Maharbiz, "Can we build synthetic, multicellular systems by controlling developmental signalling in space and time?", *Current Opinion in Chemical Biology*, 2007, vol. 11, pp. 604 - 611, 2007.

[124] E.M. Lucchetta, J.H. Lee, L.A. Fu, N.H. Patel and R.F. Ismagilov, "Dynamics of Drosophila embryonic patterning network perturbed in space and time using microfludics", *Nature*, vol. 434, pp. 1134 – 1138, 2005.

[125] Y. Kawakami, A. Raya, C. Rodriguez-Esteban and J.C.I. Belmonte, "Retionic acid signalling links left-right asymmetric patterning and bilaterally symmetric somitogenesis in the zebrafish embryo", *Nature*, 2005, vol. 435, pp. 165 - 171, 2005.

[126] F.J. Vonk and M.K. Richardson, "Developmental biology: Serpent clocks tick faster", *Nature*, vol. 454, pp. 282 - 283, 2008.

[127] K-S Huang, Y-C Lin, K-C Su and H-Y Chen, "An electroporation microchip system for the transfection of zebrafish embryos using quantum dots and GFP genes for evaluation", *Biomedical Microdevices*, vol. 9, pp. 761 - 768, 2007.

[128] K.M. Rambabu, S.H. Narayana Rao and N.M. Rao, *BMC Biotechnology*, 2005, vol. 5, pp. 362 – 368, 2005.

[129] P.F. Lurquin, "Gene transfer by electroporation", *Molecular Biotechnology*, vol. 7, pp. 5 - 35, 1997.

[130] M. Swartz, J. Eberhart, G.S. Mastick and C.E. Krull, "Sparking new frontiers: using in vivo electroporation for genetic manipulations", *Dev. Bio.*, vol. 233, pp. 13 - 21, 2001.

[131] H. Pauly and W.P. Schwan, "Dielectric properties and ion mobility in erythrocytes", *Biophys. J.*, vol. 6, pp. 621 – 639, 1966.

[132] K.S. Cole, *Membranes, Ion and Impulses*, University of California Press, Berkeley, 1972.

[133] T.Y. Tsong, T.T. Tsong, E. Kingsley and R. Siliciano, "Relaxation phenomena in human erythrocyte suspensions", *Biophys J.*, vol. 16, pp. 1091 – 1104, 1976.

[134] D.L. Farkas, R. Korenstein and S. Malkin, "Electroluminescence and the electrical properties of the phtosynthetic membrane", *Biophys. J.*, vol. 45, pp. 363 – 373, 1984.

[135] D. Gross, L.M. Loew and W.W. Webb, "Optical imaging of cell membrane potential changes induced by applied electric fields", *Biophys. J.*, vol. 50, pp. 339 – 348, 1986.

[136] G.A. Cerda, J.E. Thomas, M.L. Allende, R.O. Karlstrom and V. Palma, "Electroporation of DNA, RNA and morpholinos into zebrafish embryos", *Methods*, vol. 39, pp. 207 – 211, 2006.

[137] A.J.H. Sale and W.A. Hamilton, "Effects of high electric fields on microorganisms. I. Killing of bacteria and yeast", *Biochim, Biophys.Acta*, vol. 118, pp. 781 - 788, 1967.

[138] A.J.H. Sale and W.A. Hamilton, "Effects of high electric fields on microorganisms. III. Lysis of erythrocytes and protoplasts", *Biochim. Biophys.Acta*, vol. 163, pp. 37 - 43, 1968.

[139] B.L.M. Hogan, R.S.P. Beddington, F. Constantini and E. Lacey, CSH Press, New York, 1994.

[140] D.A. Kane and C.B. Kimmel, "The zebrafish midblastula transition", *Development*, vol. 119, pp. 447 - 456, 1993.

[141] T. Bansal, M.P. Chang and M.M. Maharbiz, "A class of low voltage, PDMS-gold 'wet' actuators for use in high-density microfluidics", *Lab Chip*, vol. 7, pp. 164 – 166, 2007.